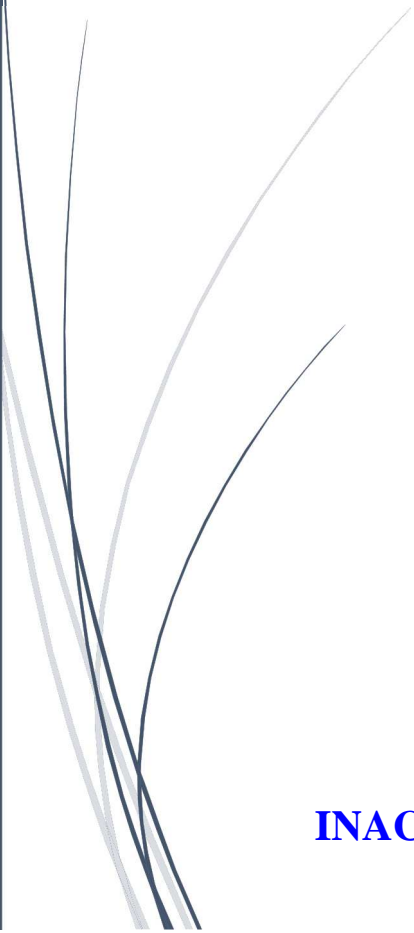
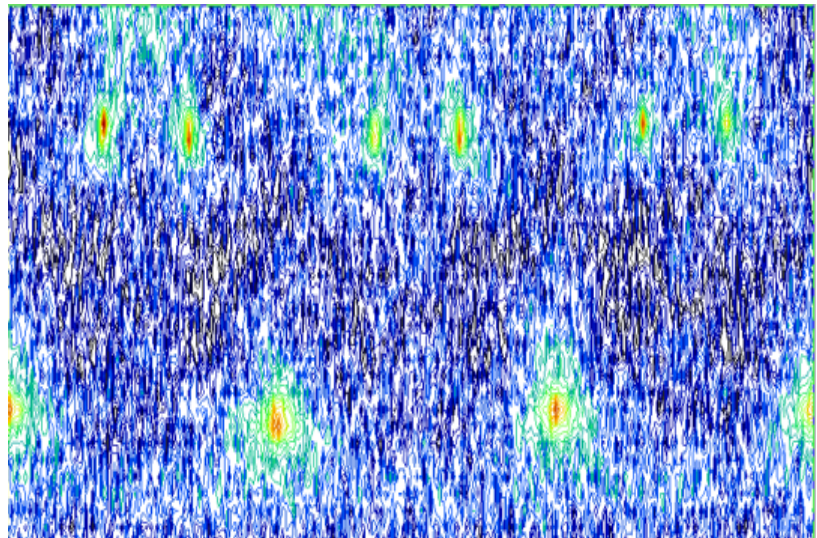
A dark grey vertical bar runs down the left side of the page. A blue arrow points to the right from the bar, positioned above the title.

SGX Activity Report 2015 -2016

Several thin, grey, curved lines originate from the bottom left corner and extend upwards and to the right, resembling stylized grass or reeds.

INAC X-Ray characterization laboratory

SGX Team

♣ Edith Bellet-Amalric (1/2 SGX -1/2 Pheliqs/NPSC)

♦ Alain Farchi

♣ Arnaud de Geyer

♦ Stéphane Lequien

♣ Bernard Mongellaz

♦ Jacques Pécaut (SyMMES/CIBEST)

♣ Stéphanie Pouget (resp.)

The SGX X-ray characterization laboratory at CEA-INAC provides access to state-of-the-art equipments, holds trainings in different fields of X-ray characterization (powder XRD, thin film XRD, reflectivity, single crystal XRD, small angle scattering), and offers advice and technical assistance in data collection and data analysis. Our facility opens to all INAC members, as well as, under conditions to be discussed, to external users.

The 2015-2016 period was marked by the arrival of the smartLab diffractometer, in the frame of the PHENIX Lanef project. This instrument is jointly managed by Institut Néel and INAC.

The undertaken upgrade of the SAXS camera was continued with the installation of rails to facilitate the changes of the sample-detector distance. A collaboration with the ILL-ESRF PSCM laboratory allowed to equip the instrument with a 2D Vantec-2000 detector.

A temperature stage was developed and installed on the powder X'Pert diffractometer. It allows measurements up to 400°C, in reflection geometry.

Contents

SGX Team	2
Instruments	
In-Plane/Out-of-Plane diffractometer (Smartlab Rigaku)	9
Small angle scattering instrument	10
Powder diffractometer (Panalytical X'Pert)	11
Thin film diffractometer/reflectometer (Panalytical Empyrean)	11
Single crystal diffractometer (Rigaku XCalibur S)	12
LAUE equipment for single crystals characterization and orientation.....	12
Software	13
Training	14
Spintronics	
Skymions in FeGe	17
Spin-to-charge conversion by Rashba coupling in metallic states at the Fe/Ge(111) interface	18
Thin films for spintronic devices.	19
Nanoelectronics	
Intersubband transition in non-polar GaN/(Al)GaN heterostructures for short-, mid- and long- infrared regions	23
Hybrid lead halide perovskite materials for optoelectronic applications	25
Characterization of NbN and NbTiN thin films for single-photon detectors	27
Energy	
Molecular hole-transporting material for solid state dye-sensitized solar cells.....	31
Chalcopyrite CuFeS ₂ nanocrystals for thermoelectrical applications.	32
Structure and Dopant Engineering in PEDOT Thin Films: Practical Tools for a Dramatic Conductivity Enhancement	34
Thermotropic ionic liquid crystals as lithium-ion battery electrolytes	35
Microporosity of hard carbons for sodium-ion batteries: relationship between the structure and the electrochemical performances	36
Graphene frameworks for enhanced energy storage.....	38
Environment / Catalysis	

SAXS investigation of mesoporous silicas: sensors for the detection of volatile compounds by optical transduction.....	43
Characterisation of silver nanoparticles accumulated in the microalgua <i>Coccomyxa actinabiotis</i> ...	44
Graphitic carbon nitride.....	45
Metallo-cyclic clusters.....	57
New « knewman-kwart » type rearrangement.....	46

Material synthesis / structuration

Control of the catalyst dewetting in the VSS growth of nanowires.....	51
Layer-structured transition metal dichalcogenides	52
Cu ₂ ZnSnSe ₄ thin films grown by molecular beam epitaxy	53
Single crystal quality checking using Laue X-ray experiment.....	54
Mott insulator compounds – new materials for resistive memory (RRAM).....	56
Magnetocaloric materials garnets and pyrochlores for adiabatic refrigeration 1 K – 4 K.....	57
Lamellar phase exfoliation	58

Metrology

Patterned membranes	63
---------------------------	----

Instruments

(Technical resp. B. Mongellaz)

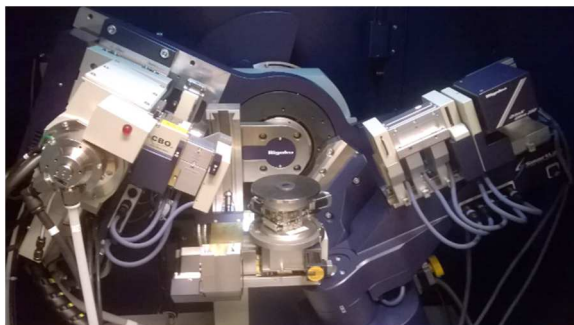
In-Plane/Out-of-Plane diffractometer (Smartlab Rigaku)

In March 2015 a new X-ray diffractometer Smartlab from the Japanese company RIGAKU arrived in the laboratory and was open to users in September 2015. The versatility of the instrument can adapt to the diversity of samples and problems specific to the field of crystalline layers of high structural quality and also to nano-crystalline objects.

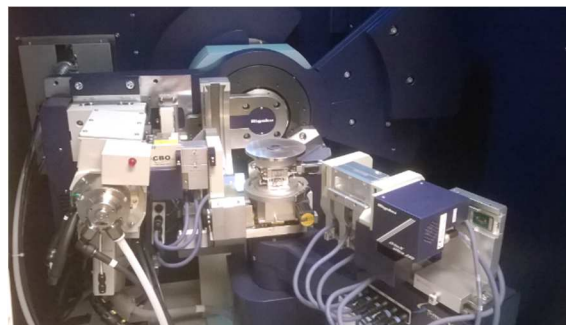
This project was carried out by Institut Néel and INAC with co-funding of the LABEX LANEF. The equipment is managed jointly by the 2 institutes. In 2016 a management agreement was signed by UGA (representing the LABEX), CEA-INAC and CNRS-NEEL. The first user meeting and steering committee were held in November 2016.

The main characteristics of the instrument are:

- High brilliance with a 9kW rotating copper anode
 - The possibility of carrying out diffraction measurements for which the diffraction vector is either normal to the surface of the sample or in the plane of the sample and more generally the ability to probe along almost any direction of the reciprocal space. For this purpose, the arm carrying the detector has two degree of freedom.
 - A modular design for an easy change of diffraction geometry:
 - High resolution mode with a parabolic mirror, 2 monochromators Ge(220) 2 and 4 reflections, a Ge(220) 2 reflections analyzer.
 - Medium resolution with a parabolic mirror and plane collimators
 - Two detectors: a punctual scintillator and a 1D strip. This linear detector allows a factor 50 in gain of time for the acquisition of reciprocal space maps.
 - A goniometer with a θ - θ configuration (horizontal sample). The motors ω , ϕ , χ , and the 2 degrees of freedom of the detector 2θ and $2\theta\chi$ allow to perform diffraction measurements in and out of plane. An independent double tilt is used for sample alignment.
 - An oven that can reach 1100°C under vacuum or under N₂ atmosphere (fix or scanning flux)
- Concerning High-Resolution X-ray Diffraction (HRXRD) it is mainly used for semiconductor materials, with different geometries: 2D thin-film or superlattices, but also in 1D nanowire geometry, or 0D quantum dots. The aim is to precisely determine the crystalline and structural properties (crystalline phase, epitaxial relations, distortions of the crystal lattice, elastic or plastic relaxation, etc.) which greatly influence the physical properties.
(*resp. E. Bellet-Amalric*).



Out-of-Plane configuration



In-Plane configuration

Small angle scattering instrument

Instrument is mounted on an *FR591-Nonius* copper rotating anode. It is equipped with Kirkpatrick-Baez mirrors with total reflection, Xenocs anti-scattering slits and 2D gas detectors (Xe/CO₂) with window of 20 x 20 cm for ESRF model and 14 x 14 cm for VANTEC-2000 model. It can accommodate various sample environments allowing *in-situ* or *operando* studies. The available flux on the sample is $\sim 3 \times 10^7$ ph/s with a beam size $\sim 600 \mu\text{m} \times 600 \mu\text{m}$, and a low angular divergence (0.05 mrad). The sample to detector distance is variable from 10 cm to 4 m, corresponding to wave vectors from 10^{-3} \AA^{-1} (SAXS domain) to 4 \AA^{-1} (WAXS domain).

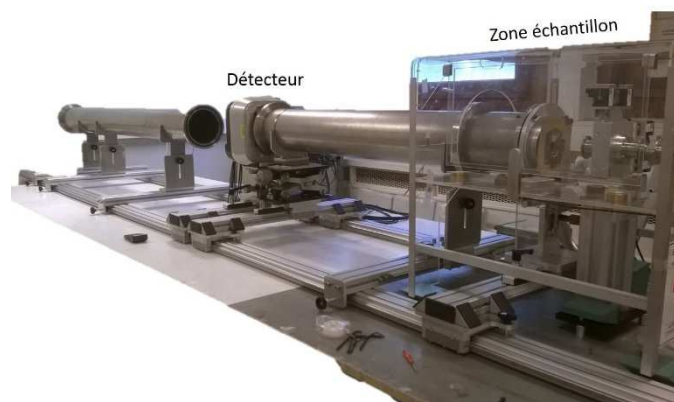
In the period 2015-2016 major developments were carried out on the SAXS instrument as part of a modernization project. This evolution has been achieved in different stages:

- non-diffusing anti-scattering slits (Xenocs slits) have been installed. Being controllable, they simplify the procedure of adjustment of the beam and of securing it. These non-diffusing slits also provide better collimation of the X-ray beam without parasitic diffusion by the edges of the slits. This advantage makes possible a better measurement quality as close as possible to the axis of the direct beam.

- a system of rails has been installed to allow rapid and easy movement of the detector along the beam axis (from 10 cm to 4 m from the sample).

- in the frame of a partnership with PSCM (ILL/ESRF) laboratory, the SAXS camera has been equipped with a VANTEC detector which was previously used on an ESRF beamline. The VANTEC-2000 detector has a $14 \times 14 \text{ cm}^2$ window and can be used with different pixel sizes (60 μm , 120 μm , 180 μm). This detector is complementary to the large (20 cm x 20 cm) gas detector already installed on the SAXS camera. MikroGap® technology gives a very fine Point Spread Function which allows to measure even weak scattering intensities close to strong peaks. The high resolution of the detector benefits SAXS measurements on systems with large correlation distances as exemplified in this report with a patterned membrane as reference sample.

(resp, A. de Geyer and A. Farchi)



Powder diffractometer (Panalytical X'Pert)



Upgraded in 2012, it is equipped with a copper anode, a 15 positions sample changer and an X'Celerator 1D detector. The diffractometer is mainly used in reflection Bragg-Brentano geometry with fixed or variable divergence slit. The sample holder can also be positioned in transmission mode especially for the investigation of membranes, with possibility to control the rotation angle in the sample plane.

Temperature stage up to 400°C.

=> Phase identification, lattice parameters and microstructure (strain, crystallite size) determination, structure refinement on polycrystalline compounds – degree of crystallinity of anisotropic polymeric membranes

(*resp. S. Pouget*).

Thin film diffractometer/reflectometer (Panalytical Empyrean)



Diffractometer equipped with a cobalt anode (Co $K_{\alpha 1}$ radiation prevents from fluorescence for samples containing iron and cobalt) and a chi, phi, z sample stage with RX, RY cradles for thin film alignment. It can be used in either diverging, parallel or mixed configuration.

Parallel geometry: Goebel mirror, long plate collimator, proportional punctual detector.

Diverging geometry: Divergence and anti-scattering slits, 2D 255x255 pixels Pixel detector (can be used in 0D, 1D or 2D mode).

=> Determination of the structure, orientation and microstructure (perpendicular and lateral strain and crystallite size) in polycrystalline, textured or epitaxial thin films.

=> Thin film reflectivity for thicknesses ranging from a few up to a hundred nanometers

=> Investigation of rough polycrystalline samples (using parallel geometry)

(*resp. S. Pouget, S. Lequien*).

Single crystal diffractometer (Rigaku XCalibur S)

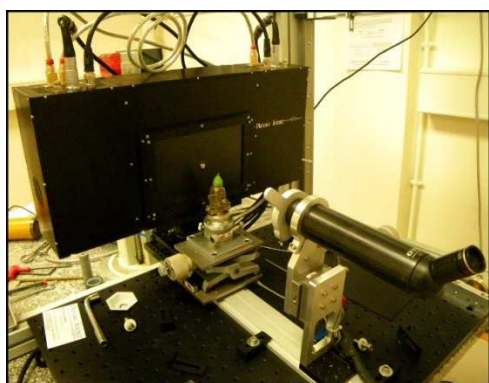


Rigaku XCalibur S (2008) equipped with a Molybdenum anode and a 4048x4048 pixels CCD detector. Nitrogen sample colling ($T > 100\text{K}$) is available.

The aim of single-crystal diffraction is the determination of the chemical composition and the atomic positions, without pre-requisite such as the formula. The obtained information are: obviously the nature of the synthesized compound (formula, charge, bond type, absolute configuration ...); however results are only typical of the chosen crystal and not of all the species present in the solution. Second, the conformation and the 3 dimensional arrangement of the chemical entities inside the crystalline lattice (hydrogen bonds, pi-pi interactions ...). For some studies, only the nature of the synthesized compound is relevant, and, in this case, crystallization is a way to reach it, while for others, interest is not focused only on the motive structure (asymmetric unit) but also on the interactions between the different entities in the cell.

(*resp. J. Pécaut*).

LAUE equipment for single crystals characterization and orientation



The X ray source is a SIEMENS Kristalloflex generator K760 1.8 kW (45 kV – 40 mA) equipped with a polycapillary XOS™ optic especially designed for focusing and collimating the incident X ray beam. Laue patterns are recorded with a dual camera from Photonic Science™ through PSL software, and Orient Express, free software for indexation and matrix orientation.

(*resp. G. Lapertot INAC/PHELIQS/IMAPEC*)

Software

The laboratory provides users with different specific analysis programs.

- **ICDD PDF-4** : Data base for crystalline phase identification from experimental powder pattern.
- **HighScore Plus** : phase identification – lattice parameters determination – size/strain analysis - Rietveld refinement.
- **FullProf** : advanced Rietveld refinement.
- **X'Pert Epitaxy**: strain and stoichiometry determination in epitaxial thin films and super-lattices.
- **Motofit, Parratt, GenX**: reflectivity - simulation and refinement.
- **CCDC/Mercury** : Cambridge data base of single-crystal structures, and visualization.
- **Olex** : interface for structure resolution and finalization of publication files.
- **ShelX 2013** : structure resolution with direct methods, structure refinement.
- **Superflip** : « charge flipping » structure resolution method.
- **Platon** : diffused solvents modelization (SQUEEZE).
- **MPAWIN** (Fast ComTec): SAXS data treatment and reduction.
- **Datasqueeze**: SAXS data analysis (for different particle and interaction models).
- **PDXL** :basic treatment of diffraction data.
- **3D Explore** : visualization and analysis of reciprocal space maps and pole figures.
- **SmartStudio2** : simulation of diffraction data for thin films and super-lattices. It allows to simulate diffraction pattern for any crystalline or semi-crystalline inorganic material, to define the axis of growth and the state of relaxation of the successive layers.

Training

SGX holds trainings in different fields of X-ray characterization; they are validated by the physics and chemistry doctoral schools.

- Single crystal diffraction
- Polycrystalline materials
- Thin film characterization – from powder...to single crystal epitaxial layer.
- High resolution thin film diffraction
- Small Angle X-Ray scattering

Spintronics

Skyrmions in FeGe

INAC/SPINTEC

We are interested in magnetic materials in which a skyrmion phase could be present under specific temperature and magnetic field conditions. One of those is FeGe, in the B20 non-centrosymmetric cubic structure. But the crystalline quality is essential to allow the existence of skyrmions. We have grown FeGe films by high temperature sputtering, which were then characterized by X-ray diffraction. These measurements confirmed the presence of FeGe B20 crystalline phase with two different textures, $\langle 111 \rangle$ and $\langle -1 -1 -1 \rangle$. These two growing directions are non-equivalent due to the chirality of the structure.

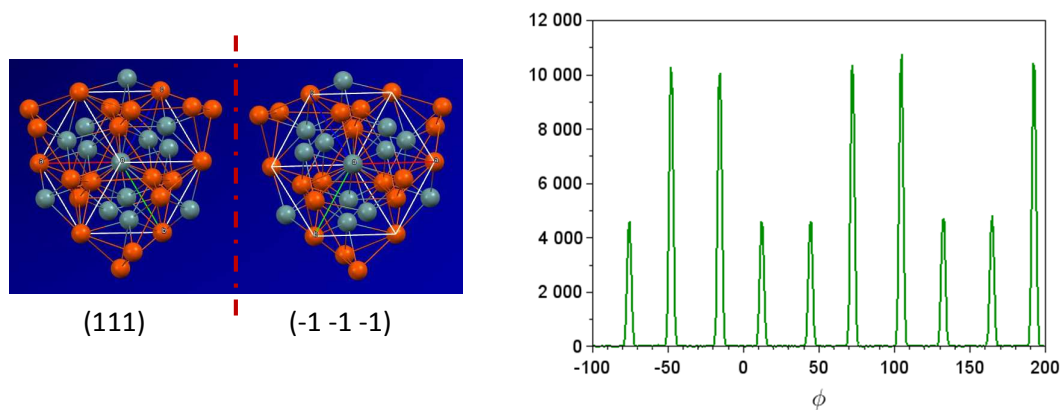


Figure 1 : Left side, representation of (111) and (-1 -1 -1) planes for the B20 structure of FeGe, using Mercury software (the red dotted line represents the plane of symmetry). This clearly illustrates the non-equivalence of the two growing directions.

Right side, azimuthal scan for the (410) Bragg reflection. The fact that diffraction peaks are observed every 30 degrees implies the presence of both $\langle 111 \rangle$ and $\langle -1 -1 -1 \rangle$ textures.

Skyrmions can also appear in another type of samples which are multilayers of a magnetic material sandwiched between two heavy metals (with high spin-orbit coupling). For this purpose we sputtered Au/Co/Pd multilayers. Since the thicknesses of the layers and the roughness of the interfaces are critical to obtain the good ratio between the magnetic interactions (anisotropy, Dzyaloshinski Moriya interaction and exchange), we performed X-ray reflectivity, which is a very powerful technique to characterize multilayers.

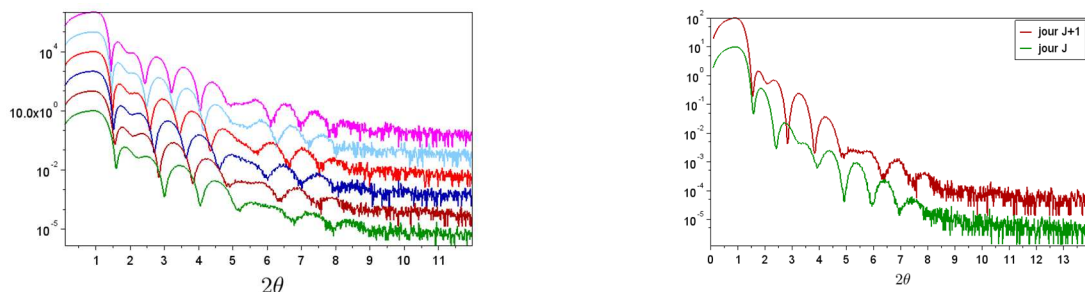


Figure 2 : On the left, different reflectivity curves along the tantalum wedge (from 8 to 11 nm).

On the right, 24h apart reflectivity measurements of one zone of the wedge. The increase of the tantalum oxide thickness is obvious.

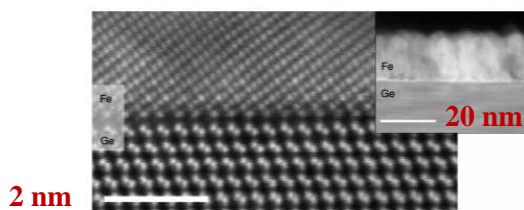
To control the thickness of the magnetic layer, we tried to grow wedges, starting with a monolayer of tantalum to calibrate our sputtering machine. Then we achieved reflectivity along the wedge of Ta (see Fig 2 left). By accident we also noticed a change in the reflectivity patterns over time (see Fig 2 right), letting us quantify the oxidation velocity of the tantalum around one day long.

Spin-to-charge conversion by Rashba coupling in metallic states at the Fe/Ge(111) interface

Coll. INAC/SPINTEC

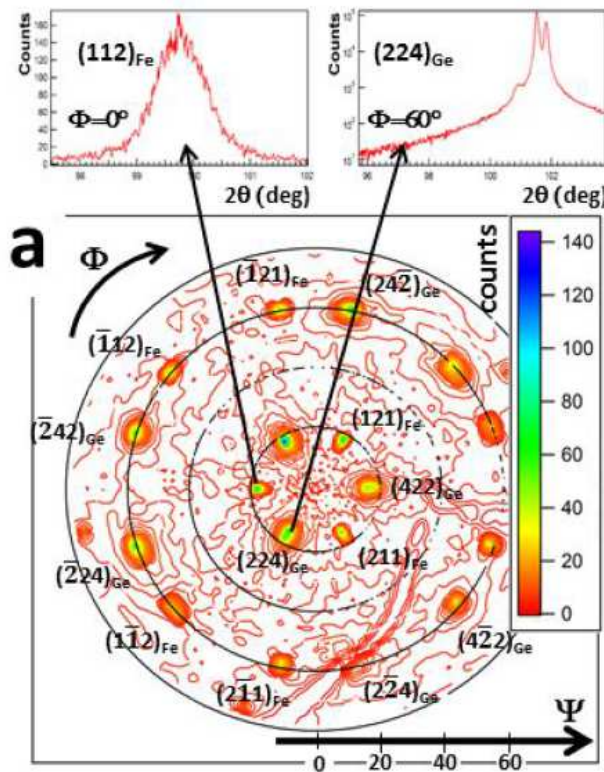
Today the field of spintronics mainly relies on the exchange coupling in ferromagnetic materials to generate and detect spin-polarized currents. However, the spin-orbit coupling appears now as a very efficient way to complete both operations. Indeed, it has been shown that spin-polarized currents can be generated and detected by the spin Hall effect in bulk materials and the Rashba effect at interfaces. Both effects concern semiconductors in which they have first been observed, but also heavy metals, alloys or metallic interfaces. One of the Graal of spintronics is the spin field-effect transistor which requires the spin injection, manipulation and detection at room temperature in Si or Ge. Although the spin Hall effect is very weak in bulk germanium it can be strongly enhanced at the interface between Ge(111) with heavy metal due to the Rashba effect.

For the purpose of the study, Fe thin films were grown on Ge(111) by molecular beam epitaxy, and characterized by X-ray diffraction and scanning transmission electron microscopy. It was shown that the Fe layer grows epitaxially on Ge(111) with [111] texture and a 60° rotation around [111] with respect to Ge planes. The epitaxial relationship is thus $\text{Fe}(111)[11-2] // \text{Ge}(111)[2-1-1]$.



High resolution scanning transmission electron microscopy image of the Fe/Ge(111) interface in cross-section along the [0-11] Ge crystallographic axis.

The Fe/Ge(111) interface was then investigated. A giant spin-to-charge conversion due to the Rashba effect into spin-split metallic states was observed, despite the relative lightness of Fe and Ge atoms. First-principles electronic calculations confirmed the presence of these metallic states at the Fe/Ge(111) interface.



XRD $\{211\}$ pole figure for $2\theta=99.8^\circ$ with a 3° detector angular acceptance. Φ and Ψ are the azimuth and declination angles respectively. $(112)_{\text{Fe}}$ and $(224)_{\text{Ge}}$ $\omega/2\theta$ scans are also presented.

♠ Evidence for spin-to-charge conversion by Rashba coupling in metallic states at the Fe/Ge(111) interface. S. Oyarzun, A.K. Nandy, F. Rortais, J.-C. Rojas-Sanchez, M.-T. Dau, P. Noël, P. Laczkowski, S. Pouget, H. Okuno, L. Vila, C. Vergnaud, C. Beigné, A. Marty, J.-P. Attané, S. Gambarelli, J.-M. George, H. Jaffrès, S. Blügel & M. Jamet. *Nat. Commun.* **7**, 13857 (2016)

Thin films for spintronic devices

INAC/SPINTEC

One of the fields of Spintronics concerns the development of new materials to be grown in multilayer structures combining ferromagnetic materials, heavy metals with strong spin orbit effect and barriers. In this context, a new chamber with sputtering sources was designed and connected to the (SP2M/NM now SPINTEC) MBE machine in order to add new synthesis possibilities such as CoFeB, Ta, MgO etc.

These materials need structural characterization. Reflectivity measurements are performed to calibrate layers thicknesses but also to characterize the growth quality. For instance, Figure a shows the reflectivity on a Ta layer sputtered on SiO₂. The simulation shows that a thin Ta oxide layer must be taken into account. Among heavy metals, bismuth shows very intriguing electronic properties. We plan to study these properties and the Rashba states as a function of the thickness. Bismuth grows epitaxially on Ge(111) at room temperature but in different phases depending on the film thickness and residual strain. We have recently shown that a new allotropic phase forms below ~ 5 nm whereas it relaxes to its bulk phase above this thickness. Figure b shows the $\theta/2\theta$ scan on a bismuth layer grown on Ge(111).

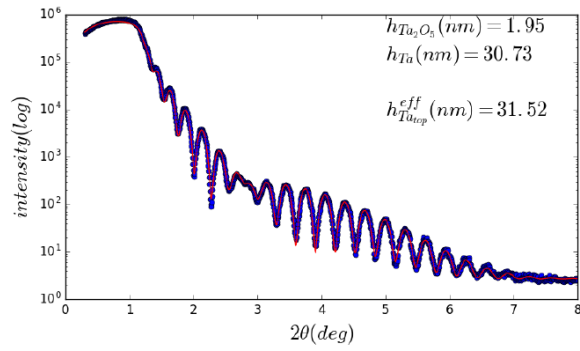


Fig. 2a: Reflectivity on Ta layer grown on SiO₂/Si substrate. The introduction of an oxide at the surface is needed to fit the spectra

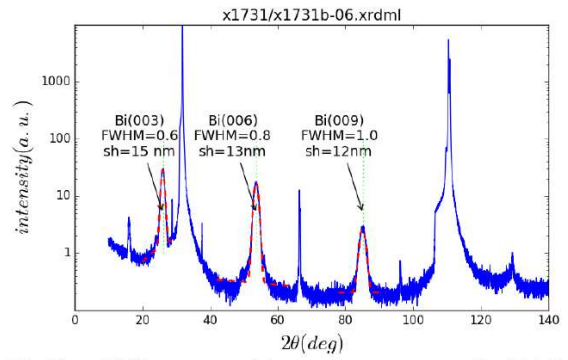


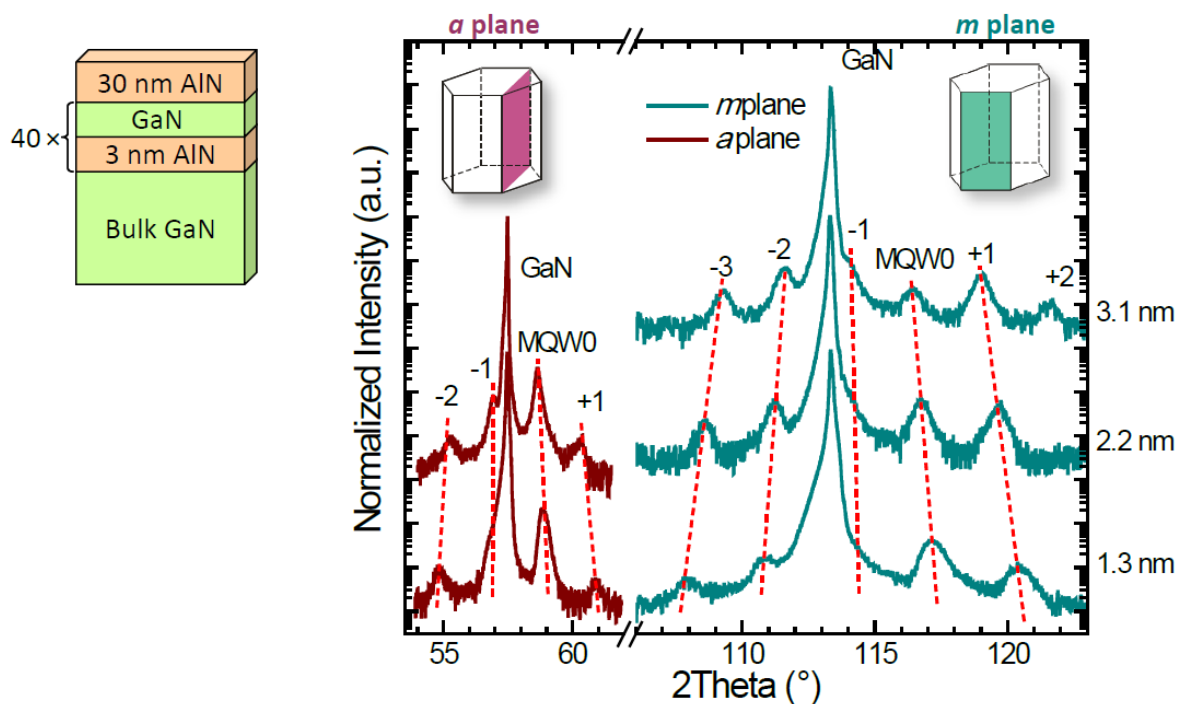
Fig2b : $\theta/2\theta$ scan on bismuth grown on Ge(111). The widths of the peaks correspond to the thickness of the layer.

Nanoelectronics

Intersubband transition in non-polar GaN/(Al)GaN heterostructures for short-, mid- and long-infrared regions

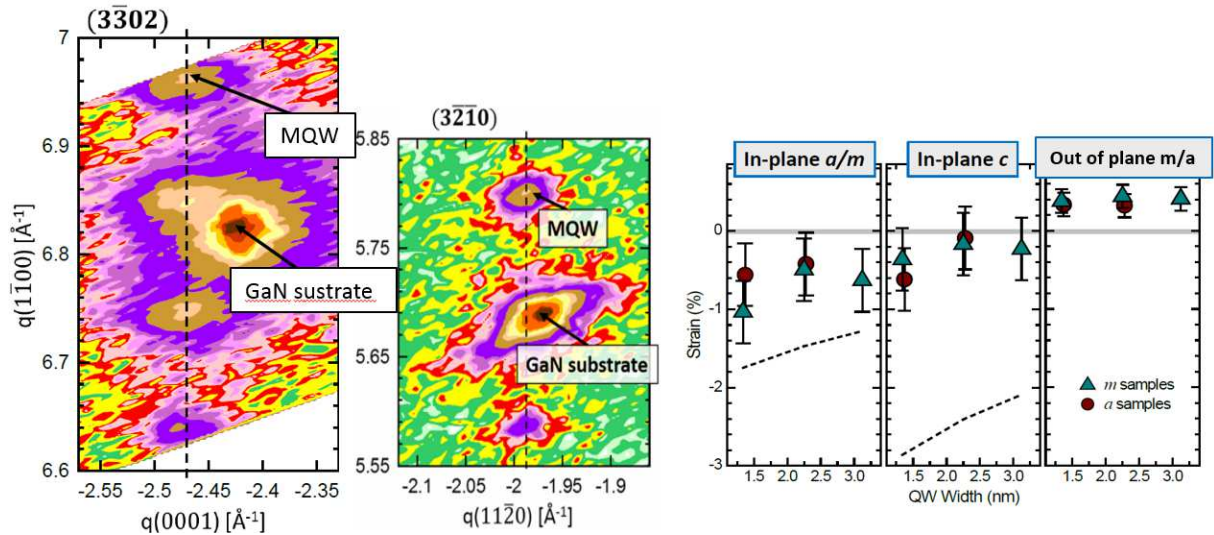
Coll. INAC/SP2M/NPSC

GaN-based nanostructures have recently emerged as promising materials for new intersubband (ISB) optoelectronic devices, with the potential to cover the whole infrared spectrum, including the 5-10 THz band inaccessible to As-based technologies. So far, research has mostly focused on the polar c-plane crystallographic orientation of GaN, in which the spontaneous polarization-induced internal electric field increases design complexity, and ultimately complicates the extension of the technology towards the THz region. With high-quality free-standing nonpolar GaN substrates being now available, the use of nonpolar crystallographic orientations can be considered as a promising alternative.

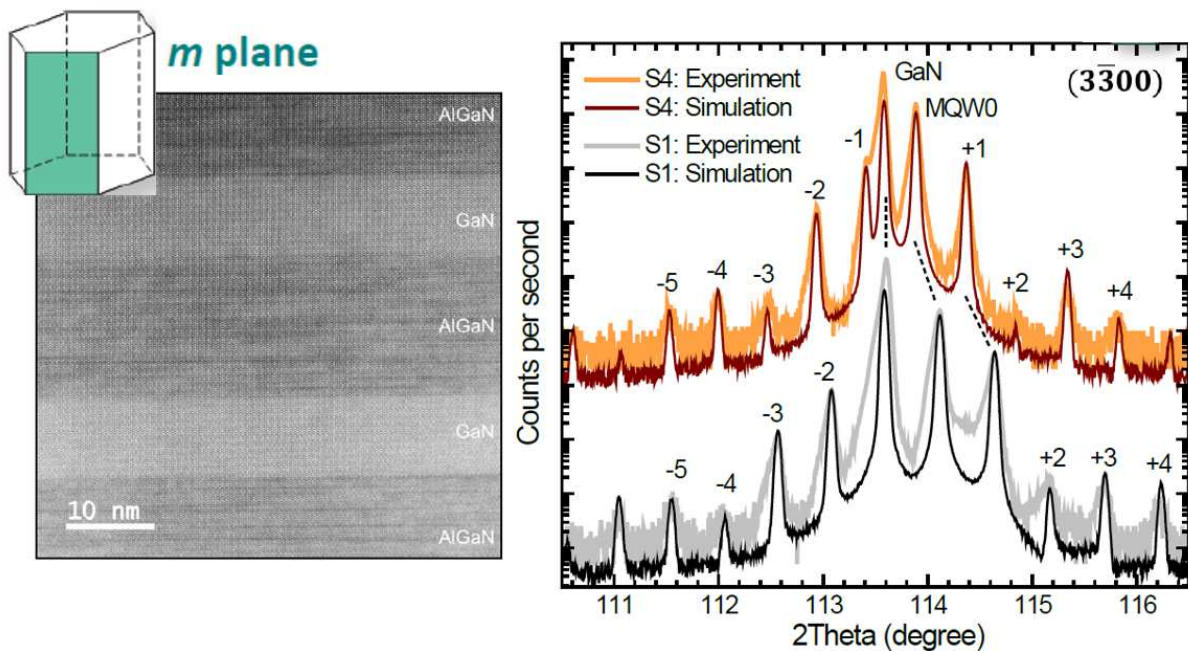


Comparison of the same non-polar structure grown on an *a*-plane and *m*-plane: XRD *q*-2*q* scans of the (3-300) reflection (*m*-plane) and the (11-20) reflection (for *a*-plane). The corresponding Quantum Well (GaN layer) thicknesses are indicated at the right of the figure.

The Rigaku SmartLab X-Ray diffractometer in a high-resolution configuration with a 4 bounce Ge(220) monochromator and a 0.114° collimator in front of the detector is a key tool for the development of this subject. Thanks to its high flux a systematic study of all the grown samples can be performed. The high resolution configuration allows to characterize the structural quality of the samples, mainly for the GaN/AlGaN multi-quantum wells. Here are some examples of the different type of studies that are regularly performed.



Measurement of the strain state of the samples: reciprocal space maps 2.2 nm thick *m*-plane sample. Left ($3\bar{3}02$) reflection with the *c*-axis in the diffraction plane. Middle ($3\bar{2}10$) reflection with the *a*-axis in the diffraction plane. Right: Strain state extracted from the XRD measurements for the two in-plane directions and for the resulting out of plane direction.



Characterization of GaN/AlGaIn *m*-plane superlattices: left by electron microscopy (HAADF-STEM image). Right by XRD diffraction. Experimental and simulated curves showing the good quality of the samples. From these two complementary techniques the thickness, concentration and relaxation state of the layers can be obtained

♠ Intersubband transitions in nonpolar GaN/Al(Ga)N heterostructures in the short- and mid-wavelength infrared regions C. B. Lim, M. Beeler, A. Ajay, J. Lähnemann, E. Bellet-Amalric, C. Bougerol, and E. Monroy *J. Appl. Phys.* 118, 014309 (2015)

♠ Effect of doping on the far-infrared intersubband transitions in nonpolar *m*-plane GaN/AlGaIn heterostructures C.B. Lim, A. Ajay, C. Bougerol, J. Lähnemann, F. Donatini, J. Schörmann, E. Bellet-Amalric, D.A. Browne, M. Jiménez-Rodríguez, and E. Monroy *Nanotechnology* 27 (2016) 145201

♠ **Short-wavelength, mid- and far-infrared intersubband absorption in nonpolar GaN/Al(Ga)N heterostructures** C. B. Lim, M. Beeler, A. Ajay, J. Lähnemann, E. Bellet-Amalric, C. Bougerol, J. Schörmann, M. Eickhoff, E. Monroy
Jpn. J. Appl. Phys. **55** 05FG05 (2016)

♠ **Effect of Al incorporation in nonpolar m-plane GaN/AlGaN multi-quantum-wells using plasma-assisted molecular-beam epitaxy** C.B. Lim, A. Ajay, C. Bougerol, E. Bellet-Amalric, J. Schörmann, M. Beeler and E. Monroy - Accepted for publication in *Phys. Status Solidi A*

Hybrid lead halide perovskite materials for optoelectronic applications

Coll. INAC/SyMMES/STEP

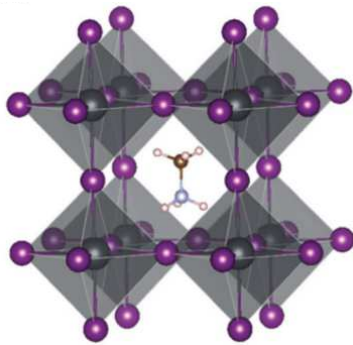


Figure 1: Schematic crystal structure of hybrid perovskite $\text{CH}_3\text{NH}_3\text{PbI}_3$ (violet: I, grey: Pb^{2+} , in the centre: CH_3NH_3^+)

Hybrid organic-inorganic lead halide perovskite solar cells have recently taken the photovoltaic research world by storm, with efficiencies above 20% achieved after only 5 years of substantial work. This new type of photovoltaic technology thus represents an alternative to the silicon and the thin films solar cells which currently lead the market. These outstanding photovoltaic performances are closely linked to the intrinsic properties of the hybrid perovskite absorber, whose key attributes include ease and low costs of fabrication, strong solar absorption and low non-radiative carriers recombination rates.

The perovskites refer to a family of compounds having a cubic crystal structure the general formula of which is ABX_3 . In the case of the hybrid lead halide perovskites materials: A is an organic cation (typically methylammonium CH_3NH_3^+), M is the lead cation (Pb^{2+}) and X is a halide anion (most often I, Br^- or Cl^-) (Figure 1). They form an octahedral structure MX_6 where M occupies the centre of an octahedron surrounded by the anions at the corners. The MX_6 structure consists of a 3D network by connecting the corners of the octahedrons. The empty space formed by eight adjacent octahedrons in the 3D network is occupied by a cation A which is thus surrounded by 12 X close neighbours. By modifying the composition of the halide perovskite, the optical and electronic properties of the materials can be easily tuned. So, depending on the halide used, the band gap can be continuously tuned from ~ 1.6 eV (pure I) to 3.2 eV (pure Cl), with the smaller bandgap materials providing better solar cell efficiencies. Even smaller band gaps can be achieved using a different organic cation (e.g., formamidinium $\text{H}_2\text{NCHNH}_2^+$) or inorganic cation (e.g., Sn) and such compounds are desirable as they have a higher efficiency limit.

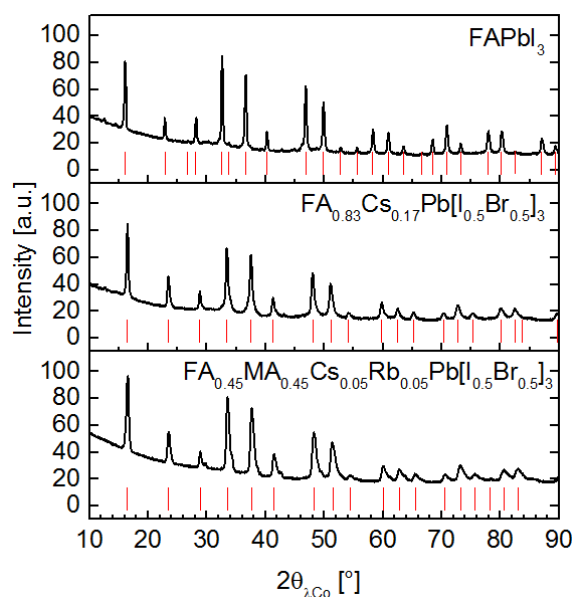
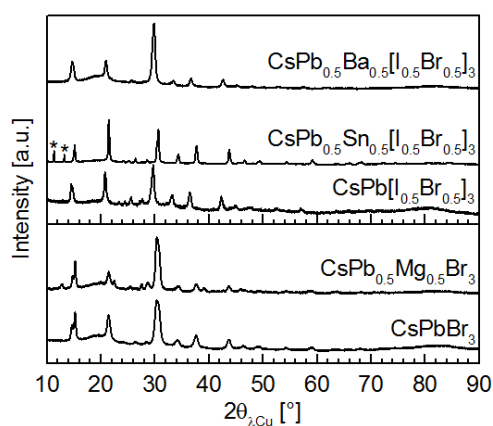


Figure 2: XRD patterns of lead halide perovskite powders based on the formamidinium cation (FA) or a mixture of organic (FA, methylammonium MA) and inorganic (Cs, Rb) cations. Le Bail profile fit of the powder diffraction patterns confirming a single tetragonal phase $I4/mcm$.

Although these perovskites have remarkable properties as solar-cells absorbers, their potential commercial implementation now requires a greater focus on the material's inherent shortcomings (e.g. degradation on exposure to moisture and ultraviolet radiation) and environmental impact (lead toxicity during device fabrication, deployment and disposal). These issues can be addressed through the design of new materials. The X-ray diffraction characterization is then used for phase identification and structure determination of new perovskite materials (partial substitution of lead, lead-free, mixture of organic cations A, ...) elaborated in the form of powders (Figure 2) or nanocrystals (NCs) (Figure 3).



Lattice parameters of synthesised NCs			
Composition	a [Å]	b [Å]	c [Å]
CsPbBr ₃	8.24(2)	11.73(2)	8.18(1)
CsPb _{0.5} Mg _{0.5} Br ₃	8.27(2)	8.27(2)	8.10(1)
CsPb[I _{0.5} Br _{0.5}] ₃	8.17(7)	11.8(1)	7.91(4)
CsPb _{0.5} Sn _{0.5} [I _{0.5} Br _{0.5}] ₃	8.76(1)	12.40(2)	8.64(1)
CsPb _{0.5} Ba _{0.5} [I _{0.5} Br _{0.5}] ₃	5.79(5)	5.79(5)	5.79(5)

Figure 3) XRD patterns of partially substituted methylammonium lead halide perovskite nanocrystals $CsPb_{1-x}M_x[I_{1-y}Br_y]_3$ with $M = Mg, Sn, \text{ or } Ba$. Le Bail profile fits of the powder diffraction patterns confirmed that most of the samples are single phase with orthorhombic symmetry (cubic symmetry for $CsPb_{0.5}Ba_{0.5}[I_{1-y}Br_y]_3$, tetragonal symmetry for $CsPb_{0.5}Mg_{0.5}Br_3$). The lattice parameters are given in the table. Only $CsPb_{0.5}Sn_{0.5}[I_{1-y}Br_y]_3$ presents impurities (denoted by *).

♠ **Direct Evidence of Chlorine Induced Preferential Crystalline Orientation in Methylammonium Lead Iodide Perovskites Grown on TiO₂.** M. Bouchard, J. Hilhorst, S. Pouget, F. Alam, M. Méndez, D. Djurado, D. Aldakov, T. Schulli, P. Reiss – Accepted in *The Journal of Physical Chemistry*

Characterization of NbN and NbTiN thin films for single-photon detectors

Coll. INAC/PHELIQS/NPSC

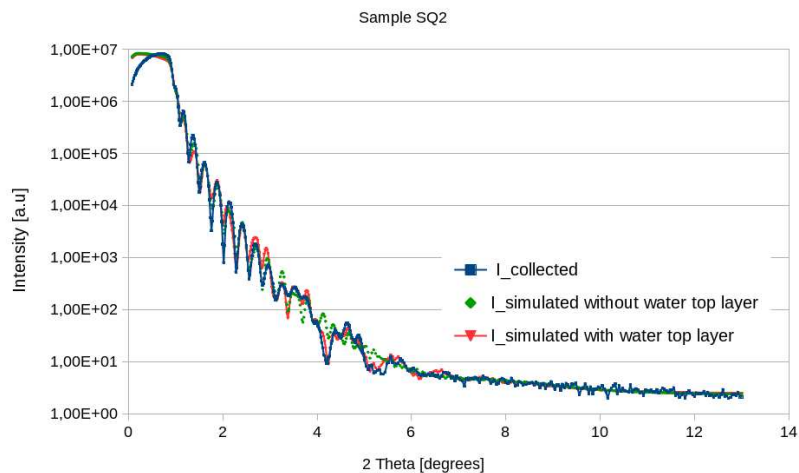
Superconducting single-photon detectors (SSPD) or superconducting nanowire single-photon detectors (SNSPD) have been developed since 15 years at visible and/or infrared wavelengths. They are single photon sensitive with recovery times and timing precision orders of magnitude faster than existing single photon detectors. Most of SNSPD are made of NbN or NbTiN which offer a relatively high critical temperature comparatively to operation that takes place at the boiling point of liquid He (4.2 K). However, when layers are processed to get SNSPD devices, some of them do not reach expected performances they have been designed for. So investigations have been performed by X-ray techniques to determine:

- the real stack of layers, their thicknesses, surface or interface roughnesses,
- the composition of NbTiN when necessary.

NbN or NbTiN layers were deposited by DC sputtering on Si (001) substrates with thermal SiO₂ layer (thickness comprised between 230 to 280 nm).

X-ray reflectivity measurements show that depending on deposition conditions, an oxide layer Nb₂O₅ occurs as soon as it is exposed to air. Although reflectivity curves could be simply adjusted with Nb₂O₅ top layers, fits can be improved by introducing transition layers NbO₂ and NbO. Their presence is corroborated by XPS measurements. A NbO_xN_{1-x} layer/interface could be envisaged but is not detectable with the operation conditions. Nb₂O₅ thicknesses evolved from 1 nm to 3 nm as a function of ageing time. On another hand, Nb₂O₅ is hygroscopic and depending on air conditions, it can be coated with a water layer (see figure).

Diffraction experiments have been carried out on NbTiN layers to check their crystallinity and therefore estimate their composition from knowledge of their lattice parameters assuming that the solid solution obeys to a Vegard's law.



Reflectivity and simulated curves for a fresh NbTiN sample

Energy

Molecular hole-transporting material for solid state dye-sensitized solar cells

Coll. INAC/SYMMES/STEP

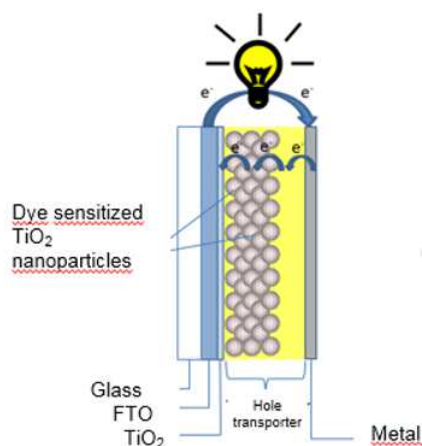


Figure 1: Schematic view of a solid state dye sensitized solar cell.

Dye Sensitized Solar Cells (DSSC) are attracting much attention because of their relatively high conversion efficiencies, low cost production processes and short energy payback time. In these devices, sunlight is absorbed by photoactive molecules that are attached to the surface of a wide band gap semiconductor oxide (typically TiO_2 or ZnO) forming a dense monolayer. The system is completed using a hole transporting material which is usually a liquid electrolyte containing the iodide/tri-iodide (I^-/I_3^-) red/ox couple. The molecules act as sensitizers and upon photo-excitation inject an electron into the conduction band of the metal oxide. While the electrons are conducted through the nanostructured metal oxide to reach the external circuit, the oxidized dye is regenerated by the red/ox couple, which is itself regenerated at the counter electrode.

Commercialization of the technology has nevertheless to face some important issues. Above all, the use of a liquid electrolyte raises limitations on the manufacturing options to provide good sealing of the cells. To overcome this issue, solid-state DSSC have been developed, in which the liquid electrolyte is replaced by a solid-state hole-transporting material, typically an organic semiconductor. In 1998, Bach and Grätzel et al. reported the first efficient solid state DSSC with amorphous organic hole transporter spiro-MeOTAD (2, 2', 7, 7' -tetrakis (N, N-di-p-methoxyphenylamine) 9, 9'-spirobifluorene). It is still the most commonly-used organic hole conductor, mainly because of its good solubility in common solvents. Nevertheless much effort has been devoted to find alternative materials to overcome its high cost and low conductivity.

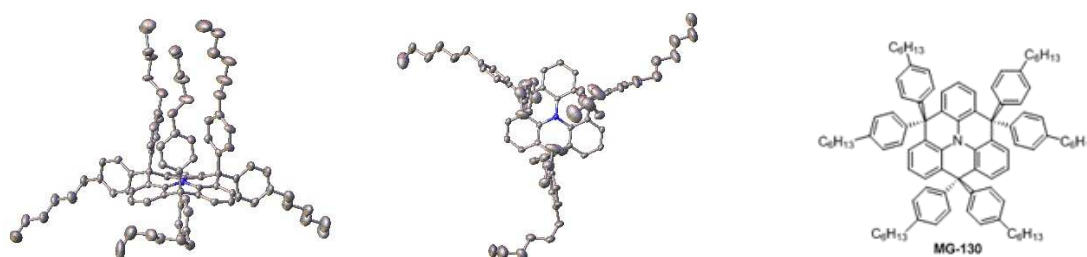


Figure 2: MG-130 crystalline structure determined by single crystal X-ray diffraction at $T=150\text{K}$

A small-molecule hole transport compound, denoted MG-130, has been synthesized at INAC/SYMMES/STEP, as single crystal, powder and thin film. The crystalline structure was

determined by single crystal diffraction at $T=150\text{K}$. The identified monoclinic space group was $P2_1/c$ with lattice parameters $a = 21.538(2)\text{ \AA}$, $b = 21.122(2)\text{ \AA}$, $c = 17.159(1)\text{ \AA}$ and $\beta = 108.215(7)\text{ deg}$. The XRD pattern obtained with MG-130 powder at room temperature was analysed with the Fullprof software. The Le Bail profile refinement confirmed the crystalline structure determined for the single crystal, with lattice parameters $a = 21.83(1)\text{ \AA}$, $b = 20.98(1)\text{ \AA}$, $c = 17.20(1)\text{ \AA}$ and $\beta = 107.61(4)\text{ deg}$. XRD measurements were then performed on a MG-130 thin film spin coated on glass substrate. Figure 4 displays a $\theta/2\theta$ scan. Only (0k0) peaks are visible, indicating a [010] texture of the film. The determination of the crystalline structure and orientation is essential as the optimization of the transport properties necessitates to control the film molecular organization.

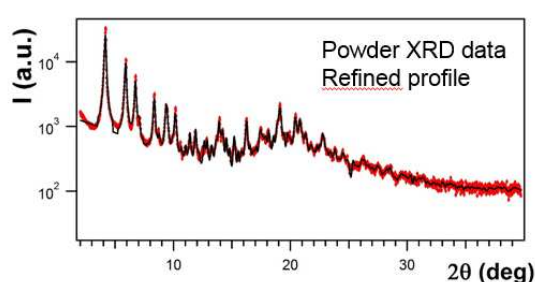


Figure 3: XRD powder pattern obtained with MG-130 powder. The black line results from a Le Bail profile refinement.

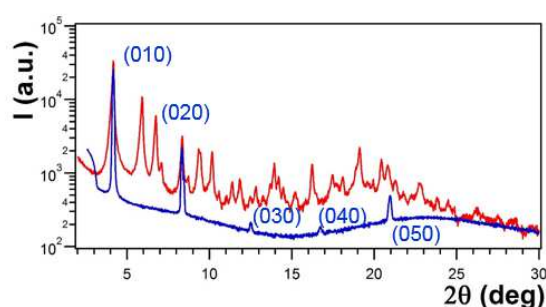


Figure 4: (blue) $\theta/2\theta$ scan measured with a MG-130 film spin coated on glass substrate. The powder pattern is shown in red.

♠ **Synthesis and characterization of a new fused triphenylamine-based molecular hole-transporting material for photovoltaic applications**, M. Mendez Malaga et al. (submitted).

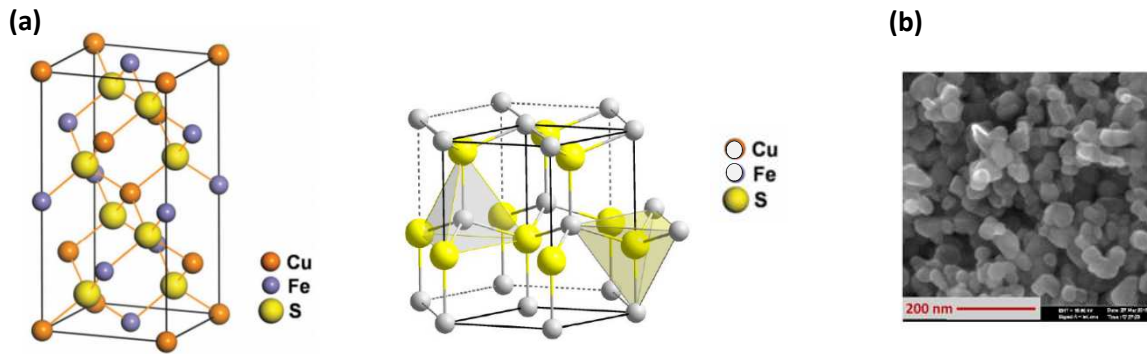
Chalcopyrite CuFeS_2 nanocrystals for thermoelectric applications

Coll. INAC/SyMMES/STEP

Owing to their ability to convert waste heat into electrical power, thermoelectricity is the subject of strong interest, and great progress has been made in improving existing thermoelectric materials. But today the best performance compounds are based on toxic or very expensive elements such as respectively Pb or Te. This contributes to their limited commercial applications. It is thus essential to focus research efforts on identifying and developing novel efficient, inexpensive and environmentally safe thermoelectric materials. Chalcopyrite CuFeS_2 is a widespread natural mineral composed of earth abundant and nontoxic elements. It is considered as a promising n-type material for thermoelectric applications. Among the different properties expected from a good thermoelectric compound, it should display high electric

conductivity and low thermal conductivity. Nano-structuration is a way of limiting phonons propagation and so thermal conductivity.

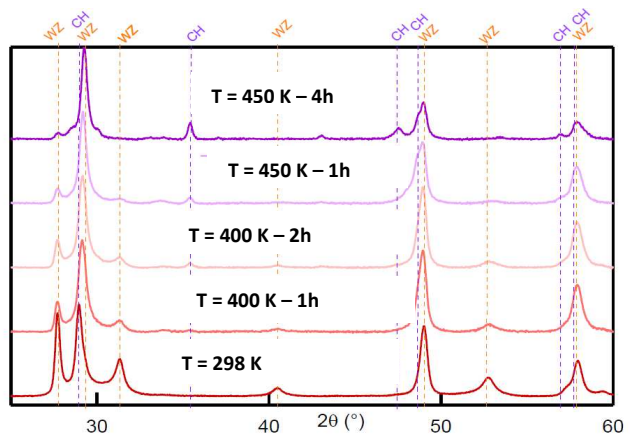
CuFeS₂ nanocrystals (nCs) were synthesized. Depending on the protocol, they appeared to be of either tetragonal or wurtzite crystalline structure. Under specific annealing conditions a phase transition between the two structures was observed.



(a) CuFeS₂ : Tetragonal and wurtzite structures.

(b) SEM image of tetragonal CuFeS₂ nCs.

Annealing induced wurtzite to tetragonal structural phase transition.



Structure and dopant engineering in PEDOT thin films: practical tools for a dramatic conductivity enhancement

Coll. LITEN/DTNM and INAC/SyMMES/STEP

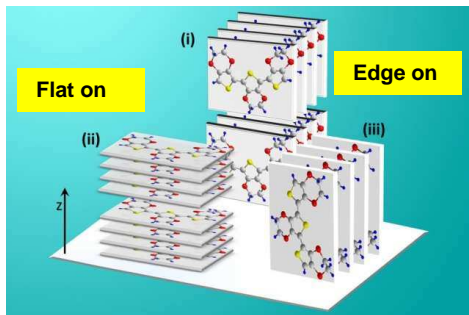


Figure 1: Typical orientations of crystalline PEDOT films.

Conductive polymers have received tremendous attention for applications in different fields such as optoelectronics or thermoelectricity due to their abundance, low cost and ease of processability. Among them, poly(3,4-ethylenedioxythiophene) (PEDOT) has focused interest owing to its stability and tunable conductivity which ranges from 0.1 Scm^{-1} for undoped PEDOT:PSS (poly(styrenesulfonate)) films up to 8797 Scm^{-1} for PEDOT monocrystals. Nevertheless there is still a large variability in reported conductivities for similar compounds, and an

exhaustive understanding of the origin of such differences is lacking. Subsequently designing optimized polymer films remains challenging.

Thin films of PEDOT stabilized with trifluoromethanesulfonate CF_3SO_3^- (OTf) counteranions (PEDOT:OTf) were synthesized. A first chemical treatment involving a high boiling point cosolvent increases the conductivity from 1200 to 3600 Scm^{-1} and further acid treatment leads to the highest conductivity ever reported for PEDOT films reaching 5400 Scm^{-1} . The PEDOT films structural properties were investigated by grazing incidence X-ray diffraction which evidences an edge-on type orthorhombic crystalline ordering. Temperature dependent conductivity experiments were performed from 3 to 315 K; they allowed to unravel the transport mechanisms which appear to be accounted for by a heterogeneous conduction model.

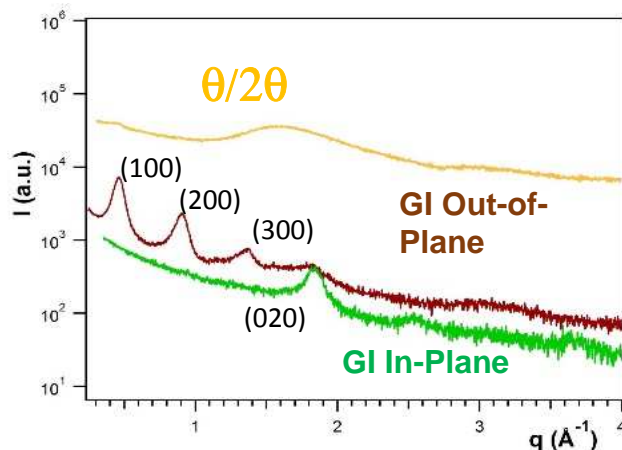


Figure 2 : XRD measurements on a 20 nm thick PEDOT layer on glass substrate. Yellow: $\theta/2\theta$ s

can mainly evidencing scattering from the amorphous substrate. brown and green: grazing incidence out of plane and in-plane scans characteristic of an edge-on orientation of the PEDOT crystalline component. The (020) peak present on the in-plane scan corresponds to π - π stacking.

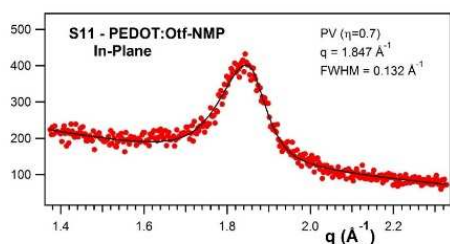


Figure 3 : Pseudo-Voigt adjustment of the π - π stacking peak measured in in-plane geometry. The values of the fitted parameters for the different diffraction peaks give access to the lattice parameters and grain size.

♠ **Structure and Dopant Engineering in PEDOT Thin Films: Practical Tools for a Dramatic Conductivity Enhancement**, M. N. Guye, A. Carella, N. Massonnet, E. Yvenou, S. Brenet, J. Faure-Vincent, S. Pouget, F. Rieutord, H. Okuno, A. Benayad, R. Demadrille and J.P. Simonato, *Chem. Mater.* **2016**, *28*, 3462-3468

Thermotropic ionic liquid crystals as lithium-ion battery electrolytes

Coll. INAC/SyMMES LITEN/DEHT

While lithium-based batteries are already the energy storage technology of choice for small- and medium-scale devices, their widespread implementation in large-scale applications like, for instance, electric vehicles remains hampered in particular by safety concerns. These concerns are, in fact, basically related to the commonly employed liquid organic electrolyte, comprising toxic, corrosive, and unstable LiPF_6 as conducting salt. In this context, INAC-SyMMES and Liten teams have developed a new generation of thermally stable, thus, intrinsically safer solid electrolyte with covalently bonded anionic functions (single-ion conductivity), showing liquid-crystalline behavior at elevated temperatures (see Fig.1).

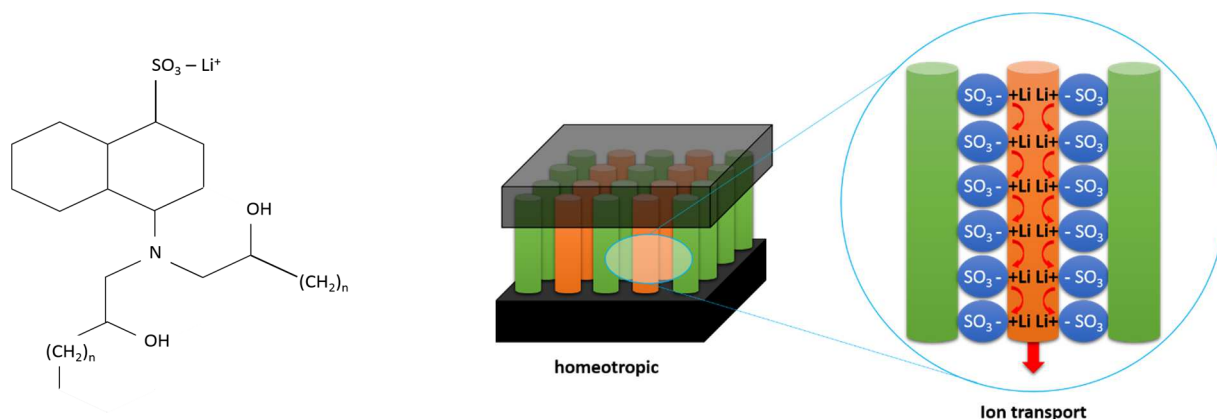


Fig1:a) CLITs ; b) Proposed a mechanism of conduction of Li^+ ions in the channels of a columnar structure.

Temperature dependent SAXS spectra of these new electrolytes were recorded in the laboratory in order to identify the different mesophases and their transition temperatures (samples in capillary between 20°C and 150°C). The structural organization of the different mesophases identified were correlated to the evolution of the conduction properties (see Fig 2).

This new family of ionic liquid crystal self-organizes in nanoscale lamellae along a columnar axis. They allow to overcome charge accumulation and thermal runaway leading to

the ignition of currently utilized liquid organic. The observed structures promote efficient ion transport and suitable thermal and electrochemical stability. The ionic conductivities and the battery performances at high temperatures are promising.

This work is continuing in the framework of a transversal thesis between Liten and Inac (L. Bernard).

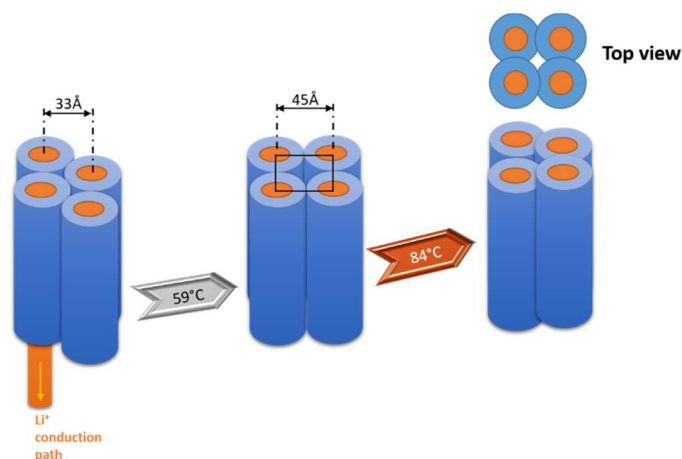


Fig. 2: Description of the mesophase transitions observed at 59° C and 84° C. for the reference ionic liquid crystal compound.

♠ **Thermotropic ionic liquid crystals as single-ion conducting lithium-battery electrolytes: investigation of the structure-transport interplay**, M. Leclere, D. Bresser, L. Bernard, P. Rannou, H. Mendil-Jakani, S. Lyonnard, L. Picard, **MRS Spring Meeting & Exhibit, Phoenix, Arizona, USA (2016)** (Oral Presentation)

♠ **Thermotropic ionic liquid crystalline polymers for lithium-ion battery electrolytes**, D. Bresser, M. Leclere, P. Rannou, H. Mendil-Jakani, S. Lyonnard, L. Picard, **228th ECS Meeting, Phoenix, Arizona, USA (2015)** (Oral Presentation)

♠ **Novel Highly Conductive Polymer Electrolytes for Li-Ion Batteries Applications** M. Leclere, H. Mendil-Jakani, P. Rannou, S. Lyonnard, S. Livi, G. Gebel, J. Duchet-Rumeau, L. Picard, **227th ECS Meeting, Chicago, Illinois USA (2015)** (Oral Presentation)

Microporosity of hard carbons for sodium-ion batteries: relationship between the structure and the electrochemical performances

Coll. LITEN/DEHT/SCGE/LGI

Today, lithium-ion batteries are used in a wide range of applications such as computers and mobile phones, and electric (EV) and hybrid (HEV) vehicles. However, the cost and accessibility of lithium resources could become a hindrance to the development of these batteries in the future. In this context, sodium-ion batteries are an interesting alternative. Hard carbon is among the most promising candidates for negative electrode materials even if its cycle

capacity needs to be improved. The role of various factors such as the microstructure of hard carbons and the various mechanisms of sodium ion insertion is still the subject of debate to establish a link between the microstructure and the electrochemical performances.

The hard carbons studied are obtained by pyrolysis of the cellulose at different temperatures (700 °C to 1600 °C). They were characterized by gas adsorption, transmission electron microscopy (TEM), powder X-ray diffraction (XRD), and small-angle RX scattering (SAXS).

The MET images and the XRD spectra give an observation of the graphene plane organization as a function of the pyrolysis temperature (disordered planes at low temperature and presence of crystallites at higher temperature) but do not provide information on the porosity of the material. Moreover, nitrogen adsorption measurements remain constrained to the only open porosity accessible to the probe molecule. The SAXS / WAXS laboratory measurements were used to characterize microporosity in the hard carbon samples (see Figure 1). The measurements show the increase in size and the decrease of the number of micropores with the pyrolysis temperature. It is observed that the best electrochemical performances are obtained for pores in a size range around 10 Å arising from pyrolysis in the range 1100 °C to 1400 °C.

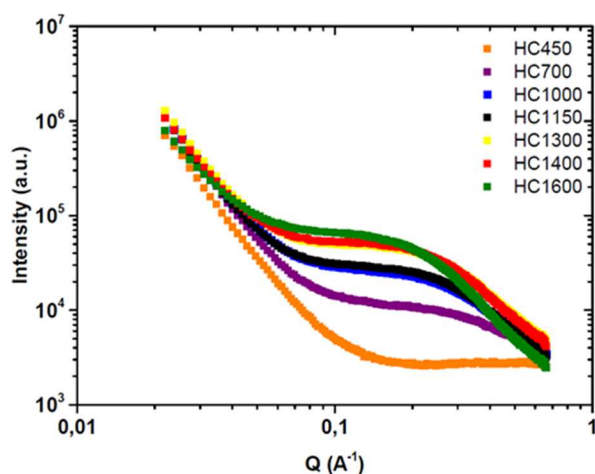


Figure 1. SAXS / WAXS curves showing the evolution of microporosity of hard carbons as a function of pyrolysis temperature ($450\text{ °C} < T < 1600\text{ °C}$). The small-angle Q^{-4} scattering part ($Q < 10^{-1}\text{ Å}^{-1}$) originates from the diffusion by the surface of the grains constituting the powder. The part of the spectra for $10^{-1}\text{ Å}^{-1} < Q < 0.6\text{ Å}^{-1}$ comes from diffusion by micropores.

This study also allows to propose a more advanced model than the "falling card model" (see Figure 2) concerning the influence of the microstructure on the insertion of sodium ions. Indeed, various insertion mechanisms can be involved and affect the electrochemical properties of the batteries differently: (1) intercalation of sodium ions between the "graphene" planes and / or (2) insertion of the sodium ions in the micropores. SAXS measurements have been carried out in the laboratory on hard carbons for different discharge potentials which should yield to discern between these different insertion mechanisms (analysis in progress).

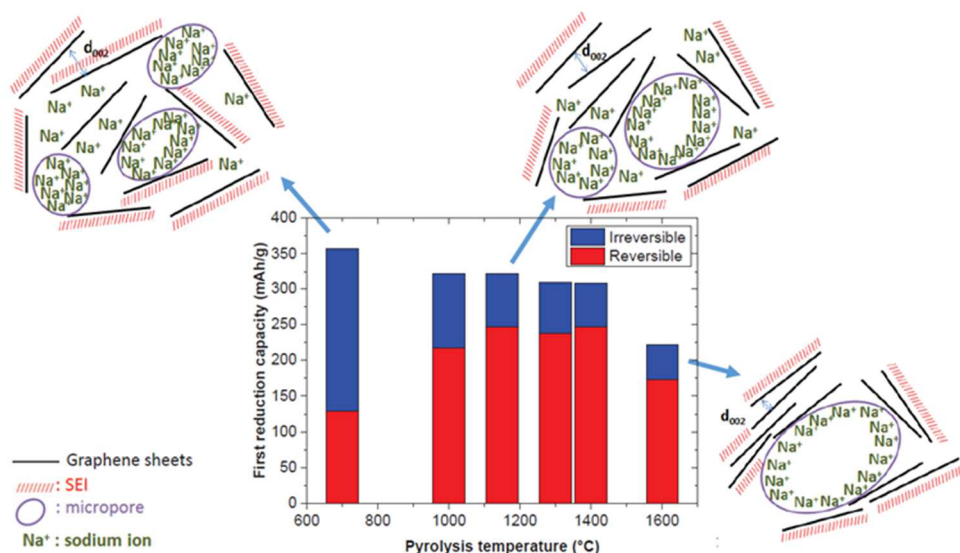


Figure 2. Simplified model (adapted from the failing card model) illustrating the effect of pyrolysis temperature on the structure and electrochemical performance of hard carbons.

♠ **Caractérisations et performances électrochimiques des carbones durs pour accumulateurs sodium-ion**, V. Simone, L. Simonin, A. Boulineau, A. de Geyer, S. Martinet, **GFECI, Autrans (2015) - oral presentation**

♠ **Hard carbons derived from cellulose as anodes for sodium-ion batteries: dependence of electrochemical properties on structure**. V. Simone, A. Boulineau, A. de Geyer, D. Rouchon, L. Simonin, S. Martinet, **J. of Energy Chemistry, 2016, 25, 761-768**

Graphene frameworks for enhanced energy storage

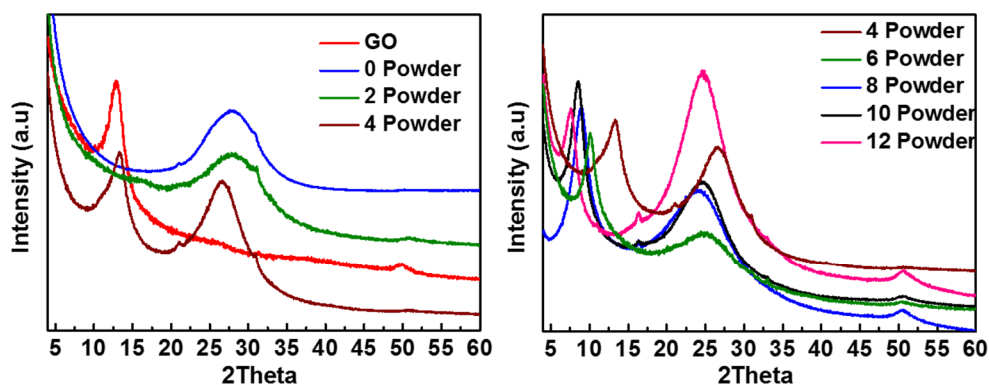
Coll. INAC/SyMMES/CAMPE

Graphene based materials have seen extensive applications in energy storage devices such as supercapacitors and batteries due to their good electrical conductivity and high surface areas. Here at SyMMES/CAMPE, we had previously been successful in synthesizing reduced graphene oxide with no metallic impurities and our partners at IMN Nantes have successfully tested such materials as conductive additives in Lithium ion batteries.

Banking on our expertise on synthesis of graphitic materials, we have now devoted our efforts towards developing tailor made graphene frameworks for supercapacitors. The challenges for graphitic materials in supercapacitors are more complex to that of batteries. From the literature, we understand that it is essential to match the electrolyte ion sizes with the pores sizes of the carbonaceous electrode materials for best supercapacitor performances. It has often been proved difficult to tune the pore sizes of carbonaceous materials with such precision. Nevertheless, recent literature suggests that the d-spacing in the graphitic frameworks could indeed be used analogous to pores in other disordered carbons. With our synthesis knowledge of graphitic materials, we believed that it is possible to tune the d-spacing in the graphitic

materials to attain a perfect match with the electrolyte ions and ensure best electrochemical performances.

Thus, XRD is an important characterization tool for our materials as we can directly access the d-spacing of the material. This would enable us to efficiently match the spacing to ion sizes in the electrolytes. Also, various equipment in INAC enable us to test both powders and aerogels. So far we have been successful in synthesizing a class of alkyldiamine assisted graphitic materials with a varying d-spacing from 3.6 Å to 13.4 Å. Currently efforts are underway to optimize the supercapacitor performances by matching d-spacing with electrolyte ion sizes.



Material	GO	0P	2P	4P	6P	8P	10P	12P
d (Å)	7.9	3.6	3.6	3.8, 7.7	3.9, 10.1	3.9, 11.4	4.0, 11.9	4.1, 13.4

XRD $\theta/2\theta$ scans measured with different compounds (GO: Graphite Oxide, 0P-12P: $(\text{NH}_2\text{---C}_n\text{---NH}_2)$ 'n' reacted powder). Due to the shape and low density of the samples the measurements are performed in transmission on the Empyrean diffractometer equipped with the mirror and the Pixcel detector. Inter-reticular distances deduced from the scans are presented in the table.

Environment / Catalysis

SAXS investigation of mesoporous silicas: sensors for the detection of volatile compounds by optical transduction

Coll. LETI/DTBS/SBSC/LCMI

Silica prepared by the sol-gel process, having a controlled porosity around 5-50 Å, are used in many applications: catalysis, selective filtration membrane, optically active layers. The LETI / DTBS laboratory is interested in the production of nanoporous silica matrices for the detection of volatile metabolites by optical transduction. The control of the size and morphology of mesopores is obtained by using alkoxy silane precursors carrying different porogenic groups (see Figure 1). Unlike the use of other molecules (surfactants, polymers), these porogenic groups are preserved after synthesis and thus participate directly in the structure while allowing control of the desired surface properties (pH, hydrophobicity / hydrophilic character). However, the role of these groups in the formation of pores is not yet fully elucidated. A better understanding of the mechanisms involved can be obtained by completing the gas adsorption (BET) studies by small-angle scattering studies that can probe structures over a wide range of distances: from nanometer to hundred nm.

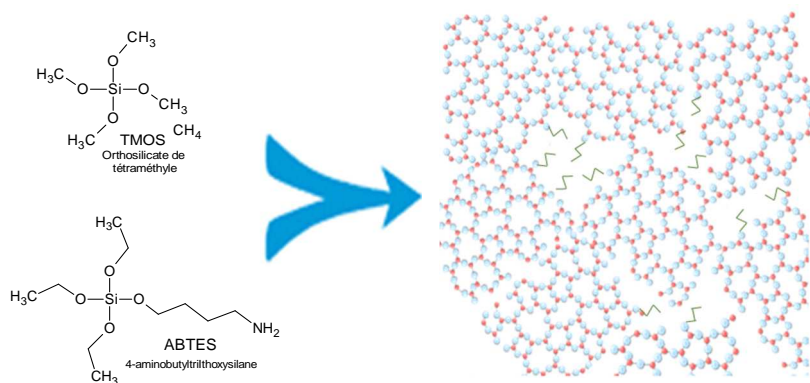


Figure 1. The mixture of the two TMOS and ABTES compounds leads in stages of hydrolysis and condensation to a xerogel of SiO₂: the ABTES groups (not involved in the hydrolysis reaction of the silica) induce the formation of mesopores.

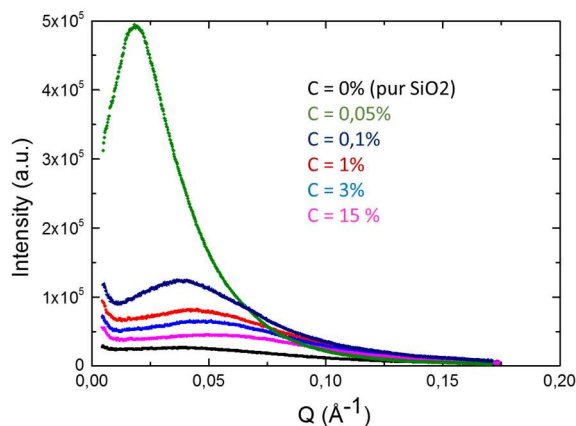


Figure 2. SAXS curves showing the evolution of silica structure as a function of the concentration of pore-forming molecule ABTES.

SAXS measurements (see Figure 2) were carried out on the silica obtained for different concentrations of porogenic molecules (from 0.05% to 15% ABTES). At a very low concentration ($C_{\text{ABTES}} \sim 0.05\%$) an intense I (Q) diffusion peak is observed, reflecting spatial correlations between well-defined diffusing objects. This concentration domain corresponds to a pore nucleation regime. In this field, the number of mesopores can grow as a function of the number of porogenic groups.

For $C_{\text{ABTES}} > 0.1\%$, the profile of the correlation peak widens and moves to the larger angles reflecting shorter interactions between less and less defined objects: this domain corresponds to a growth regime of the mesopores.

A compromise between size and number of mesopores seems to be necessary for optimization of the desired detection properties. Additional measurements will be made by SAXS to determine the maximum specific surface area that can be developed by the mesopore structure.

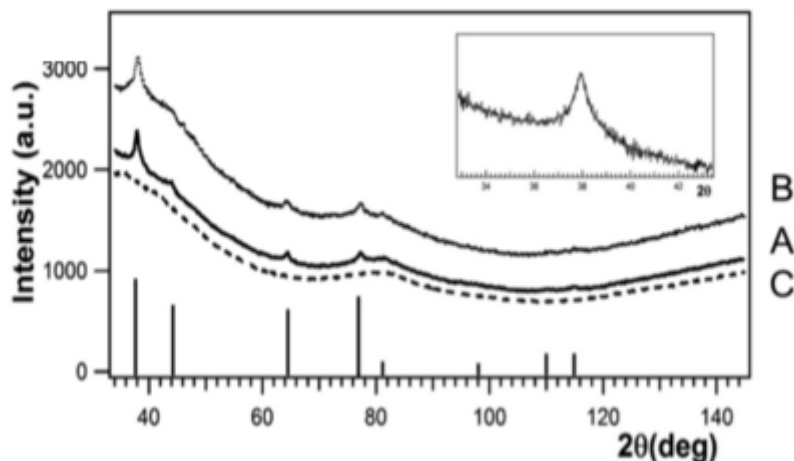
♠ **Etude de silices mésoporeuses par diffusion RX.** M. Vrignaud, A. de Geyer, S. Vignoud, P.R. Marcoux, **Rayons X et Matière, Grenoble (2015)**

Characterization of silver nanoparticles accumulated in the microalgua *Coccomyxa actinabiotis*

Coll. DRF/BIG/PCV/PLANTES_SM

Contamination of the environment by heavy metals and radionuclides is a world concern. Among these contaminants, silver constitutes one of the most toxic metals in aquatic environments. Silver toxicity depends on its speciation, the free cationic form Ag^+ being highly toxic. Remediation of effluents and of environmental water contaminated by heavy metals and radionuclides is currently mostly performed using conventional physicochemical methods, which suffer from several drawbacks such as little efficiency for the removal of very low contaminant concentrations. Biological remediation based on organisms such as bacteria, fungi and plants have offered competitive alternatives in various fields. Microalgae are good candidates for heavy metal and radionuclide bioremediation strategies owing to their ability to fix a wide range of contaminants and to resist to their toxicity.

The molecular and cellular mechanisms of silver accumulation in *Coccomyxa actinabiotis* were investigated to evaluate the potential of this promising microalgua. Silver *in situ* speciation and localization were investigated using X-ray absorption spectroscopy (X-ray Absorption Near-Edge Structure and Extended X-ray Absorption Fine Structure), X-Ray diffraction and transmission electron microscopy. It appeared that most silver is reduced to $\text{Ag}(0)$ and aggregates to form crystalline silver nanoparticles of face-centered cubic structure, with a mean size of 10 nm.



XRD data recorded for (A) solid line: microalgae exposed to 10^{-2} M Ag^+ under light, (B) dotted line: microalgae exposed to 10^{-2} M Ag^+ in the dark, and (C) dashed line: reference sample of microalgae that were not exposed to silver. Vertical unit is arbitrary, and curves were shift for clarity. The vertical lines indicate the peak positions expected for the silver Fm-3m crystalline phase taken from file 00-004-0783 of the ICDD PDF-4 database. In the inset, the fit of the (111) peak of the A sample assumes a pseudo-Voigt shape function.

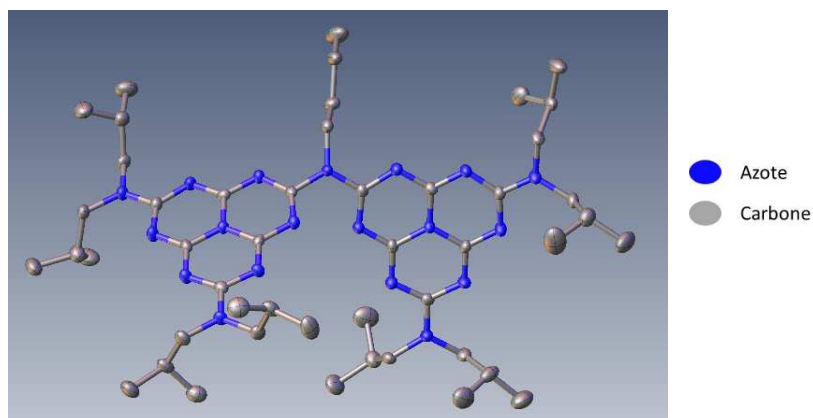
♠ **Silver accumulation in the green microalga *Coccomyxa actinabiotis*: Toxicity, in Situ Speciation, and localization investigated using synchrotron XAS, XRD and TEM.** T. Leonardo, E. Farhi, S. Pouget, S. Motellier, A.-M. Boisson, D. Banerjee, F. Rébeillé, C. den Auwer and C. Rivasseau – **Environ. Sci. Technol.** **2016**, **50**, 359-367

Structural investigation of graphitic carbon nitride

Coll. INAC/SCIB /CAMPE

Nontoxic, possibly synthesized in large amount with low cost and abundant reactants, the graphitic carbon nitride (g-CN) has an original structure with exceptional catalytic properties discovered recently. It concerns organic semi-conductor whose structure is close to graphite, with more than one carbon from two is replaced by a nitrogen. Initially studied for its catalytic properties (hydrogen production from water with visible light), the g-CN involves interesting electro-catalytic properties for dioxygen reduction. Due to its synthesis method (solid phase high temperature pyrolysis) and its physico-chemical properties (insolubility, defaults ...) precise characterization of this material is clearly challenging. Thus, property optimization and practical using are up to now limited by very few knowledge on its structure and its way of working.

In order to understand and rationalize g-CN properties, development of an original approach has been chosen: a “bottom-up” molecular approach in which the heptazine oligomers are synthesized and characterized. Models with fully defined and controlled structure allows us to understand chemical and physical defaults.



Hydrogen atoms and solvent molecules were omitted for clarity

♠ **S-Heptazine Oligomers: Promising Structural Models for Graphitic Carbon Nitride.** A. Zambon, J.M. Mouesca, P.A. Bayle, J. Pecaut, M. Claeys-Bruno, S. Gambarelli, L. Dubois, **Chem Science**, 2016,7, 945-950

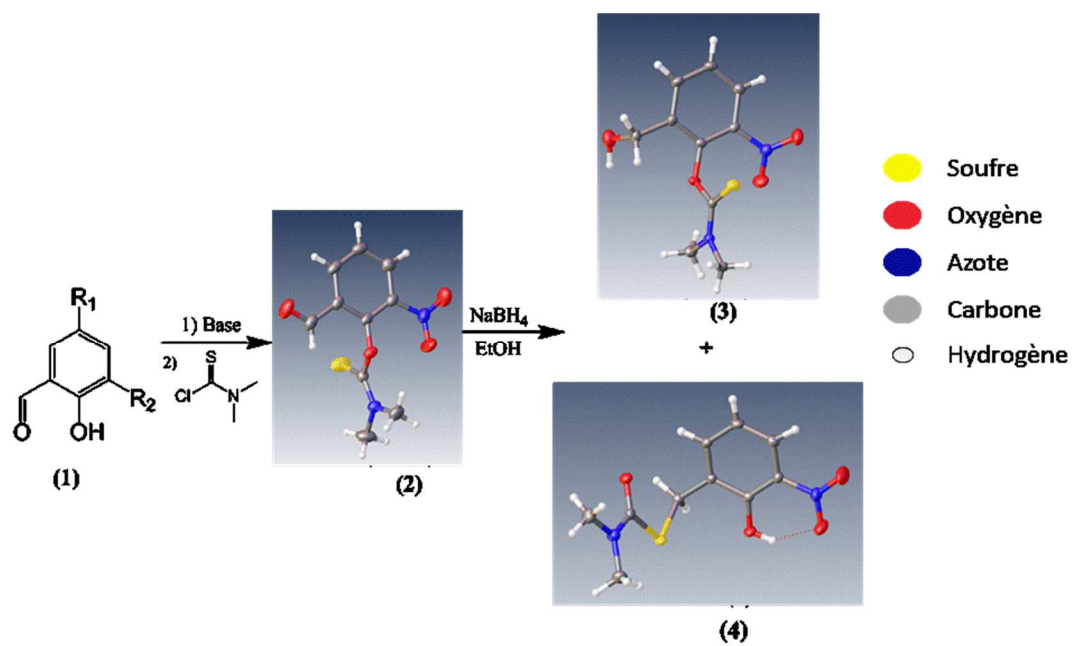
New « **knewman-kwart** » type rearrangement

Coll. BIG/CBM / BIOCE

During bio-inspired ligand synthesis for copper binuclear catalyst conception, a new type of reaction arises. Actually, reduction of a benzylic aldehyde with NaBH_4 yield to two different products. The aim was then to characterize this new chemical reaction. Therefore, five substrates were tested. It results in two final isomeric products: they have the same mass, and are not easy to distinguish with NMR. Consequently, X-ray crystallography is an ideal way to characterize two isomers.

Reactional pathway is presented figure 1: step 1 consists in the phenolate (1) attack on thiocabamyl chlorure to obtain compound (2). This one reacts in presence of reductant NaBH_4 and leads to usual reduction product (3), and the rearranged one (4).

This reaction yielding to compound 4 has been characterized through NMR, Mass and crystallographic analysis. Conclusion is that during this one and only final step, three different reactions occur: (i) thiocabamoyl group migration, (ii) aldehyde reduction, (iii) thiocarbamoyl group rearrangement. All these data evidence the increase of compound (4) synthesis due to the presence of a bulky and / or attracting group in R2 position.



Reactional pathway highlighting the molecular rearrangement.

Material synthesis / structuration

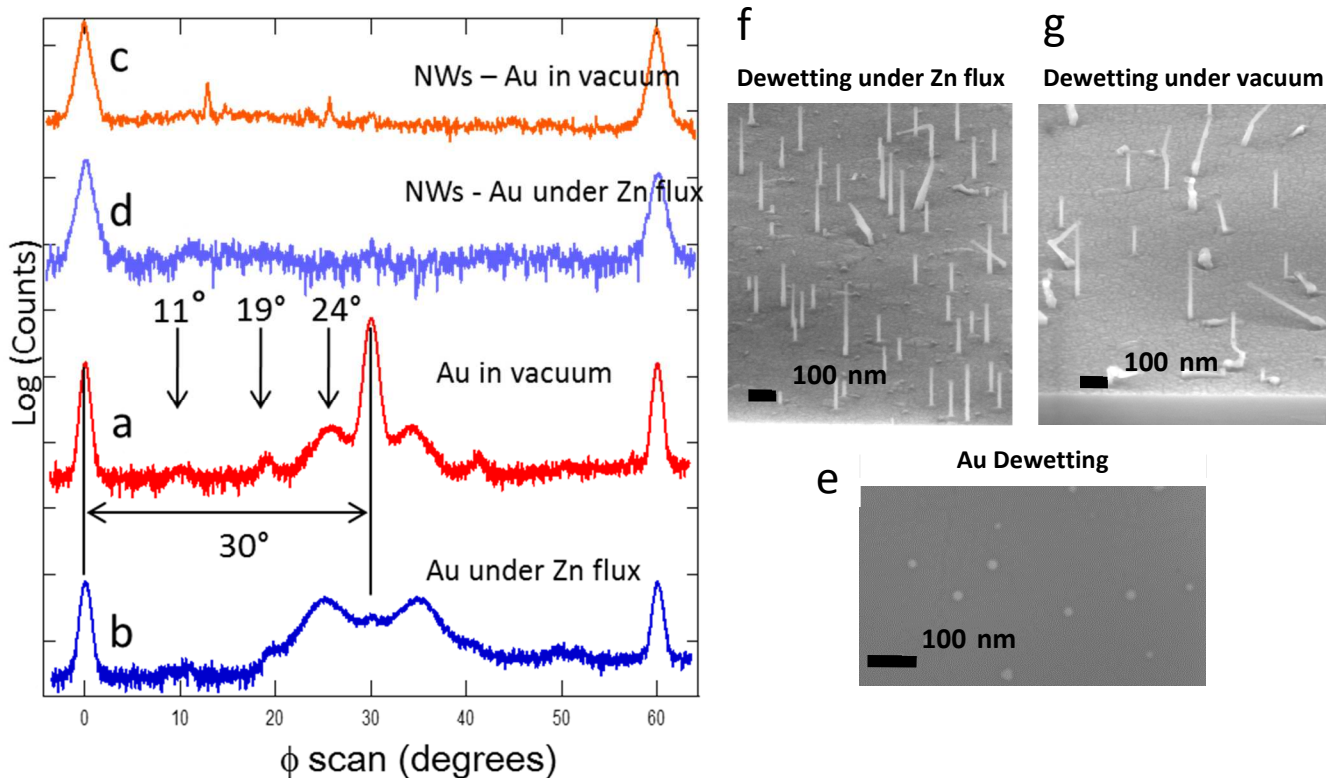
Control of the catalyst dewetting in the VSS growth of nanowires

Coll I. Néel/NPSC et INAC/SP2M/NPSC

Vapor–solid–solid (VSS) growth of nanowires is an alternative to the common vapor–liquid–solid (VLS) growth which uses a liquid catalyst. However, VSS growth still remains much less understood than VLS. In particular, the role of the catalyst nanoparticle orientation on the substrate has not been considered.

In our case we consider the growth of ZnTe nanowires on a ZnTe (111)B surface after deposition and dewetting of a sub-monolayer of Au. Thanks to the double geometry in-plane and out-of plane diffraction the use of the diffractometer Smartlab-Rigaku allows to fully characterize the epitaxial relation of the Au particles.

The Au(111) out-of-plane epitaxy is dominant ; however it presents the coexistence of up to five different in-plane orientations, one of them corresponding to the Au lattice parallel to the ZnTe lattice of the substrate (see figure). The relative intensity of the different epitaxial relationships depends on the preparation of the ZnTe (111)B surface and on the presence or not of one of the NW constituent (*i.e.*, a Zn or Te flux) during the dewetting step.



In-plane X-ray diffraction around the (220) Au reflection (Phi scans) and Scanning electron microscopy images for different samples. a, b, e: Au nanoparticles dewetted at 350°C on a ZnTe (111)B surface; c, d, f, g: ZnTe nanowires catalyzed by Au nanoparticles. a, c, e, f: dewetting the sample under vacuum, b, d, g: dewetting the sample under a Zn flux.

The $\phi = 0$ angle corresponds to the in-plane (110) direction of the ZnTe substrate. 5 different epitaxial relations are observed. After the nanowire growth only the Au nanoparticles with the same orientation as the nanowires are observed, independently of the dewetting process.

This complex dewetting process deeply influences the growth mechanism. When Au is dewetted under vacuum, a low yield of vertical nanowires (around 20%) is observed, in competition with the growth of badly formed, parasitic objects. On the contrary, dewetting under a Zn flux improves the yield of the NWs up to 80%. The direct relation between each orientation and the orientation of the nanowires is still an ongoing work. However when analyzing the Au epitaxial orientation of grown nanowires, it appears that the dominant orientation coincides with the ZnTe one.

♠ **Control of the incubation time in the VSS growth of semiconductor nanowires**, M. Orrù et al. (submitted to Applied Physics Letters).

Layer-structured transition metal dichalcogenides

Coll. INAC/SPINTEC

Layer-structured transition metal dichalcogenides (TMDs) have drawn much attention recently since they are being considered as a new class of semiconducting two-dimensional (2D) materials with thickness-tunable band-gap. In the single-layer, the TMDs offer a unique platform to explore not only the carrier transport in an ultrathin channel but also the control of 2D excitonic systems and the spin valley physics. In SPINTEC 2D team we develop Se-based 2D TMDs (MoSe₂, WSe₂, PtSe₂ etc.) grown by molecular beam epitaxy on various substrates (graphene/SiC, Pt/sapphire, muscovite etc.). Determining the crystalline orientation, strains and grain size of these layers with respect to the substrate is of great importance. Due to the 2D character of these materials, the grazing incidence in-plane diffraction mode available on Rigaku-Smartlab apparatus is well suited for such structural studies. After beam and sample alignment procedure, we determine the optimal incidence angle (in practice close to the substrate critical angle) then we proceed mainly with two type of in-plane scans:

- 1) radial scans ($2\theta_\chi/\phi$ scans) along several directions with respect to the substrate in order to determine in-plane lattice parameters, strains and correlation lengths.
- 2) azimuthal scans (ϕ scans) performed at Bragg angles found in the radial scans in order to investigate in-plane alignment and mosaic of the 2D layers with respect to the substrate.

An example of such measurements is shown on the figure below for a multilayer WSe₂/PtSe₂ grown on a Pt(111) buffer layer on the C surface of sapphire (0001).

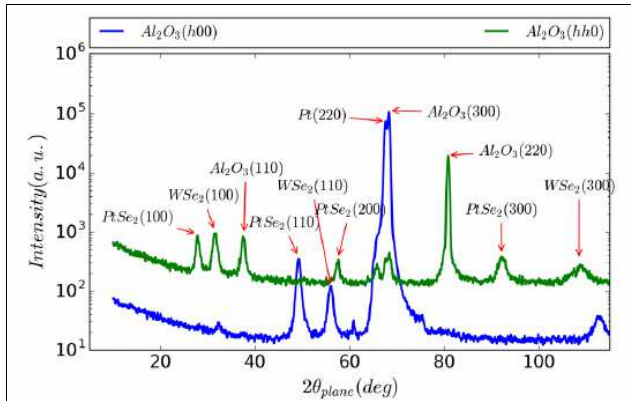


Fig. 1a :in-plane radial scan along $\langle h00 \rangle$ and $\langle hh0 \rangle$ sapphire directions.

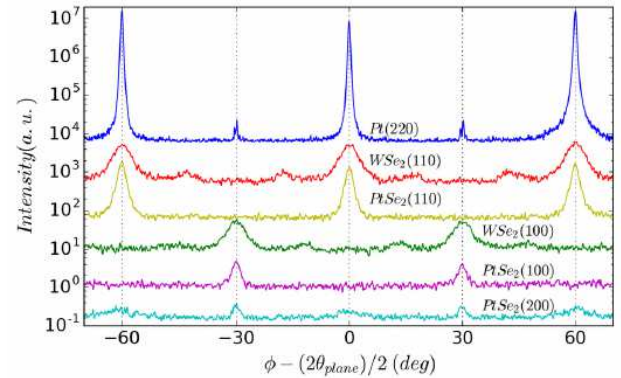


Fig. 1b : in-plane azimuthal scans for various Bragg positions of the substrate and overlayers

♠ **Layered MoSe₂ grown on sapphire by molecular beam epitaxy and its magneto-electrical properties**, M T Dau, C Vergnaud¹, A Marty, F Rortais, C Beigné, H Boukari, E. Bellet-Amalric, V Guigoz, O Renault H Okuno¹, P Pochet, M Jamet, **submitted to Appl. Phys. Lett.**

♠ **Van der Waals epitaxy of monolayer MoSe₂ on sapphire and on epitaxial graphene/SiC**

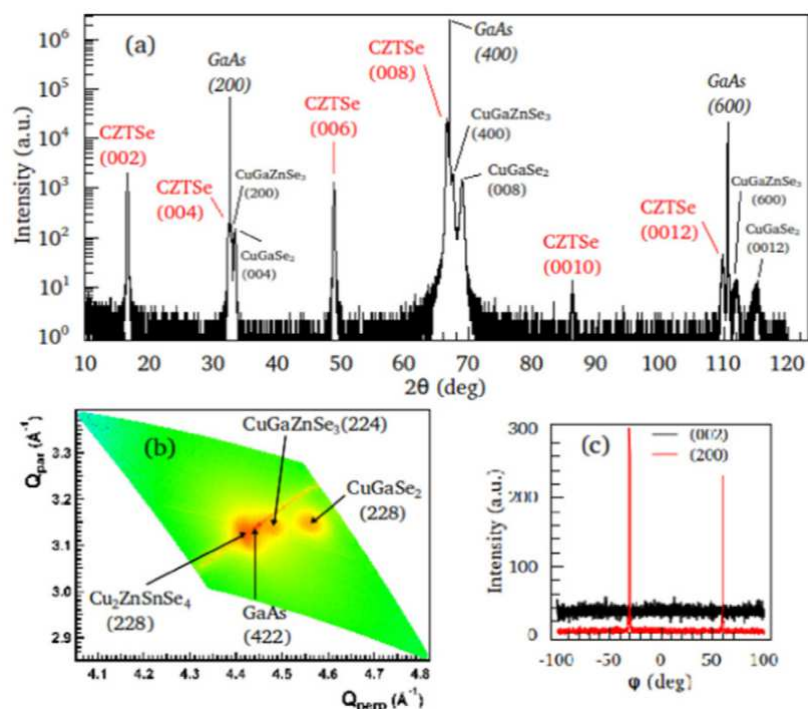
M. T. Dau, C. Vergnaud, A. Marty, F. Rortais, C. Beigné, G. Renaud, V. Guigoz, O. Renault, P. Mallet, J.-Y. Veuillen, C. Alvarez, H. Okuno, L. Huder, V. Renard, C. Chapelier, P. Pochet and M. Jamet conférence Graphene & 2D materials Montréal (Canada) October 18-20 2016 (oral contribution)

Cu₂ZnSnSe₄ thin films grown by molecular beam epitaxy

Coll. INAC/PHELIQS/NPSC

Cu₂ZnSn(S,Se)₄ (CZTSSe) is a promising compound to be used as an efficient photon absorber in thin film photovoltaic cells. Its direct and gap can be tuned in the appropriate 1-1.5 eV range, depending on the S/Se ratio. In addition, CZTSSe is composed of non-toxic and abundant elements. But fabricating single phase and stoichiometric CZTSSe is highly challenging. The compound existence domain in the phase diagram is very narrow. And indeed experimentally CZTSSe has been shown to coexist with secondary phases which contribute to the limitation of the PV cells performances. Therefore, before focusing on large-scale fabrication of CZTSSe cells one has to better understand the synthesis processes and the properties of the compound. Molecular beam epitaxy (MBE) is known to be a suited technology to fabricate high quality semiconductors and heterostructures. It is therefore an appealing approach to control the growth of CZTSSe films and allow to investigate their properties into details. MBE is definitely not suited for large-scale fabrication but it should contribute to identify the synthesis path and also the weak points of the material that have to be overcome in order to significantly improve the CZTSSe cells efficiency.

For the present study, a CZTSe film was grown on a GaAs(001) substrate by MBE. The growth was in-situ monitored by reflection of high energy electron diffraction (RHEED). The film was then characterized by X-ray diffraction and Raman spectroscopy.



(a) XRD θ - 2θ scan and (b) reciprocal space map around the GaAs(422) and $\text{Cu}_2\text{ZnSnSe}_4$ (228) reflections revealing the presence of secondary phases. (c) In-plane XRD azimuthal scans with the diffraction angle respectively set at the (002) and (200) Bragg angles. The two curves were shifted for sake of clarity. The absence of peak for the (002) scattering angle indicates a perfect [001] texture of the CZTSe film.

♠ **$\text{Cu}_2\text{ZnSnSe}_4$ thin films grown by molecular beam epitaxy.** Y. Curé, S. Pouget, V. Reita, H. Boukari, Scripta Materialia, 130 (2017) 200-204

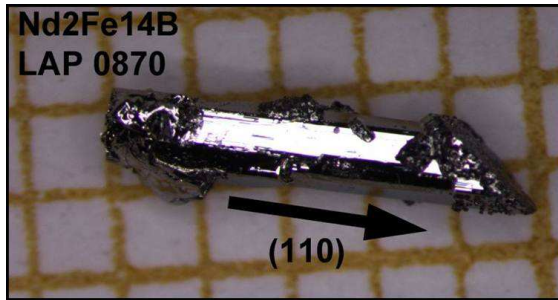
Single crystal quality checking using X-ray Laue diffraction

INAC/PHELIQS/IMAPEC

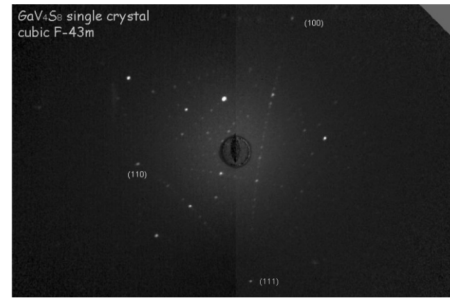
Many crystal growth experiments have been driven in IMAPEC elaboration laboratory, and have necessitated single grain confirmation and / or crystallographic matrix orientation determination. Those investigations were done after a first step of phase checking using X-ray powder diffraction.

Small single crystals

Different systems were studied using flux technique and chemical vapor transport techniques giving rise to millimetric faceted crystals: neodymium boron magnets $\text{Fe}_2\text{Nd}_{14}\text{B}$, intermetallics compounds CeAg_2Si_2 and MnSi , Mott insulators spinels GaV_4S_8 , GeV_4S_8 ...



Nd₂Fe₁₄B small single crystal, with determination of the main crystallographic directions using X ray Laue technique.



GaV₄S₈ single crystal indexed with cubic *F-43M* structure. The orientation matrix was determined explaining the triangular platelet like of single crystals, the largest surface being perpendicular to (111) crystallographic direction.

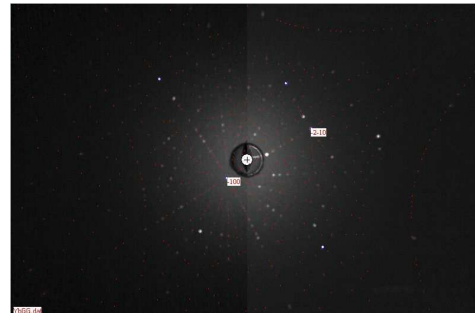
Large single crystals

Many crystal growths were performed with the travelling solvent floating zone technique, using an image furnace, giving large crystals (volume ~ cm³), typically cylindrical rod of diameter 6 to 8 mm with a length from 5 to 9 cm. Different systems of magnetocaloric garnets were investigated: Dy₃Ga₅O₁₂, Yb₃Ga₅O₁₂, Gd₃Ga₅O₁₂. Large single grains of fluoride systems, GdLiF₄ and ErLiF₄ have been also elaborated using Bridgman technique and were characterized with Laue X ray technique.

Example: Yb₃Ga₅O₁₂ large single crystal obtained by floating zone technique. Crystal quality and growth direction were investigated.



Single grain Yb₃Ga₅O₁₂ showing reversible different optical properties according post growth heat treatment under oxidizing or reducing conditions.



X-ray Laue pattern of garnet Yb₃Ga₅O₁₂ large single grain with X-ray beam along the growth direction: in those cubic systems it appears that growth direction is systematically very near (100) crystallographic axis (observed disorientation always < 8°).

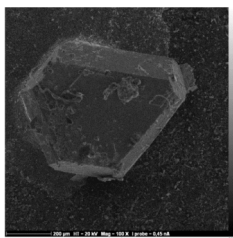
Mott insulator compounds: new materials for resistive memory (RRAM)

INAC/PHELIQS/IMAPEC and LETI/DCOS/SCME

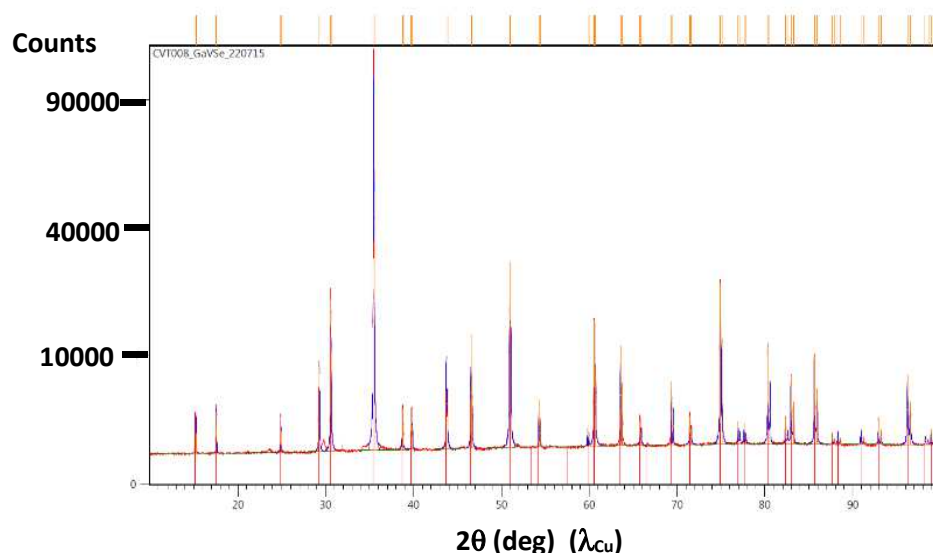
Resistive Random Access Memories (RRAM) use the large variation of resistance of a device to store 2 states of information. In several materials this change can be non-volatile, which is a strong asset for “low power” electronics.

In resistive memories based on Mott insulators, a non-volatile conductive filament is formed or disrupted in the insulating state by a voltage pulse. The mechanism could be mainly electronic, i.e. without displacement of chemical species. The main arguments supporting this assumption are the scaling of the threshold field (E_{th}) for resistive switching with the Mott insulating gap, following the same power-law as for electronic avalanche phenomena, and the 3 to 4 orders of magnitude smaller value of E_{th} compared to dielectric RRAM. Moreover, the existence of a thermodynamically stable conducting and insulating state, open the door to a resistive switching of bulk materials.

In this context, a fundamental study of the Mott-insulator mechanism in a selected family of spinel chalcogenides compounds AM_4X_8 ($A = Ga, Ge / M = V, Nb, Ta... / X = S, Se$) has been initiated in 2015. First we focused on the crystal growth of GaV_4S_8 , GeV_4S_8 , GeV_4Se_8 compounds by chemical vapor transport, in order to study the metal-insulator transition. In a second part we work on the elaboration of sulfide ceramic sputtering targets for thin films deposition using INAC-SPINTEC or LETI equipment. Each growth or steps of elaboration were checked by X ray powder diffractometer.



GaV₄S₈ single crystal obtained by chemical vapor transport with iodine, before crushing for phase and cell parameter determination. GaV₄S₈ cubic structure F-43m, cell parameter $a = 9.663 \text{ \AA}$

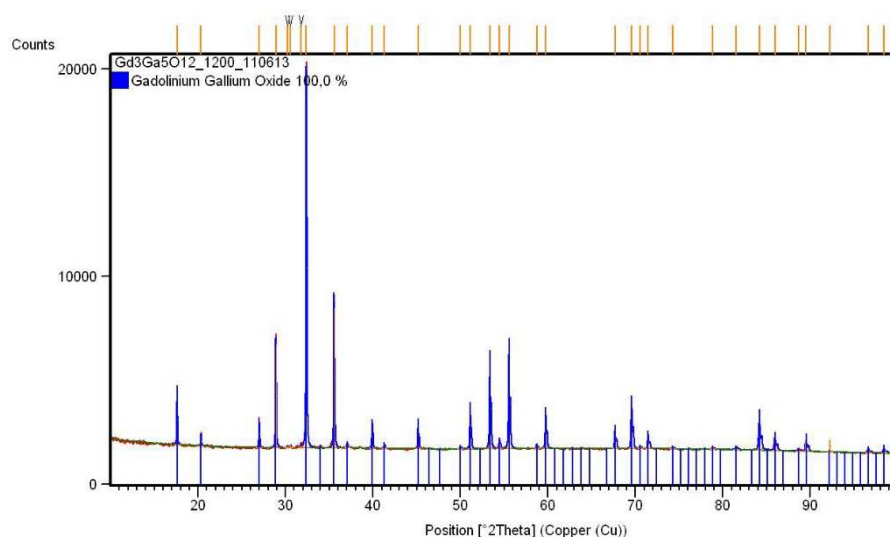


Powder diffraction pattern from crushed crystals of GaV₄Se₈ (counts in square root scale).

Magnetocaloric materials garnets and pyrochlores for 1K - 4K adiabatic refrigeration.

INAC/PHELIQS/IMAPEC and INAC/SBT/GCCS

Many magnetocaloric materials have been studied in order to optimize their magnetic properties, we spent more efforts on synthesis of ceramics and crystal growth of rare earth garnets $\text{Dy}_3\text{Ga}_5\text{O}_{12}$, $\text{Gd}_3\text{Ga}_5\text{O}_{12}$, $\text{Yb}_3\text{Ga}_5\text{O}_{12}$, but also pyrochlores $\text{Tb}_2\text{Ti}_2\text{O}_7$, $\text{Er}_2\text{Ti}_2\text{O}_7$ and fluorides GdLiF_4 and ErLiF_4 . Phase purity, crystal quality and cell parameters were checked at each steps of elaboration using X-ray powder diffractometer. Those materials were also checked using scanning electronic microscopy and were characterized with PPMS (for specific calorimetry) and MPMS (for magnetization). The final aim is to compare their magnetocaloric potential at low temperatures (1K – 4K).



Gd₃Ga₅O₁₂ powder diffraction diagram after final heat treatment at 1200°C – 2 weeks

Metallo-cyclic clusters.

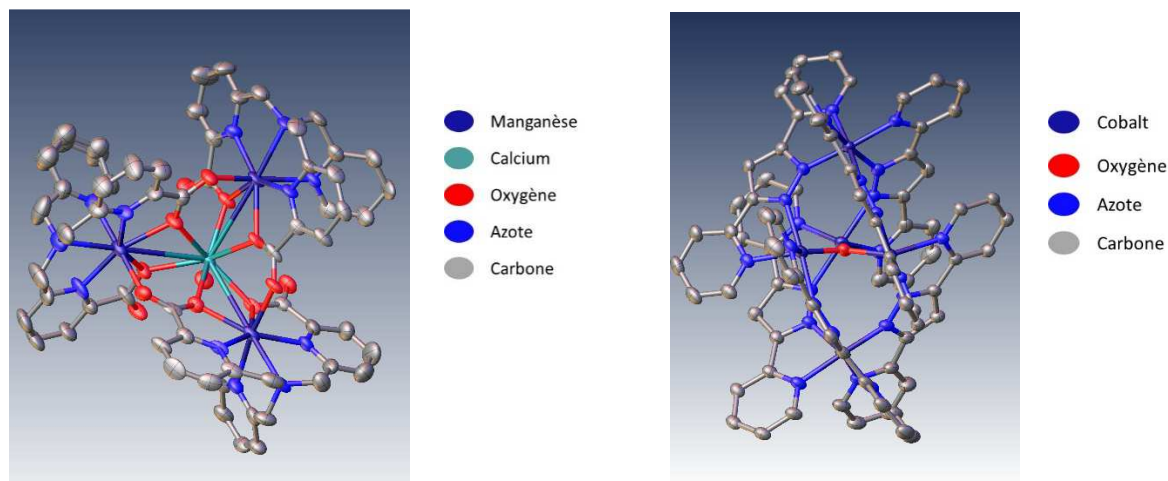
Coll. UGA/DCM /CIRE

In order to synthesize homo and heterometallic clusters, coordination of Htpada ligand has been studied in the presence of different metals (Mn, Co and Fe) in a methanol dissociating solvent. Six new structures were characterized by X-Ray diffraction, three heterometallic Mn^{3+} -X complexes (X = Li, Ca, Sr) and three homometallic M₃M ones (M = Mn, Co, Fe).

Indeed these complexes present the same metallo-cyclic architecture constituted by three metal-ligand entities, bounded by μ -carboxylato bridges, yielding to a free pocket filled by one or more cations depending on its nature (Mn_3Li_2 , Mn_3Ca or Mn_3Sr). The presence of the cation gives to the complexes a higher stability, especially in solution, allowing characterization

by several techniques. Cation nature has also a great influence on electronic and electrochemical properties, because of charge effect.

New complexes of auto assembled Co_5L_6 ($\text{L} = \text{bpp}$) pentamer type, were also characterized by X-ray diffraction. Structure analysis combined to various spectroscopies enabled to prove existence of five high spin CoII , bridged by a central μ_3 -hydroxo. Electrochemical experiments demonstrated a large compound stability for oxidation and reduction. Complex synthesis with different oxidation states ($\text{CoII}_3\text{CoIII}_2$ and CoICoII_4) were isolated and position of each oxidation or reduction (apical or equatorial) were localized.



Hydrogen atoms and solvent molecules were omitted for clarity

♠ **Manganese-calcium/strontium heterometallic compounds and their relevance for the oxygen-evolving center of photosystem II.** B. Gerey, E. Gouré, J. Fortage, J. Pécaut, M.-N. Collomb, *Coordination Chemistry Reviews* 2016, 319, 1–24

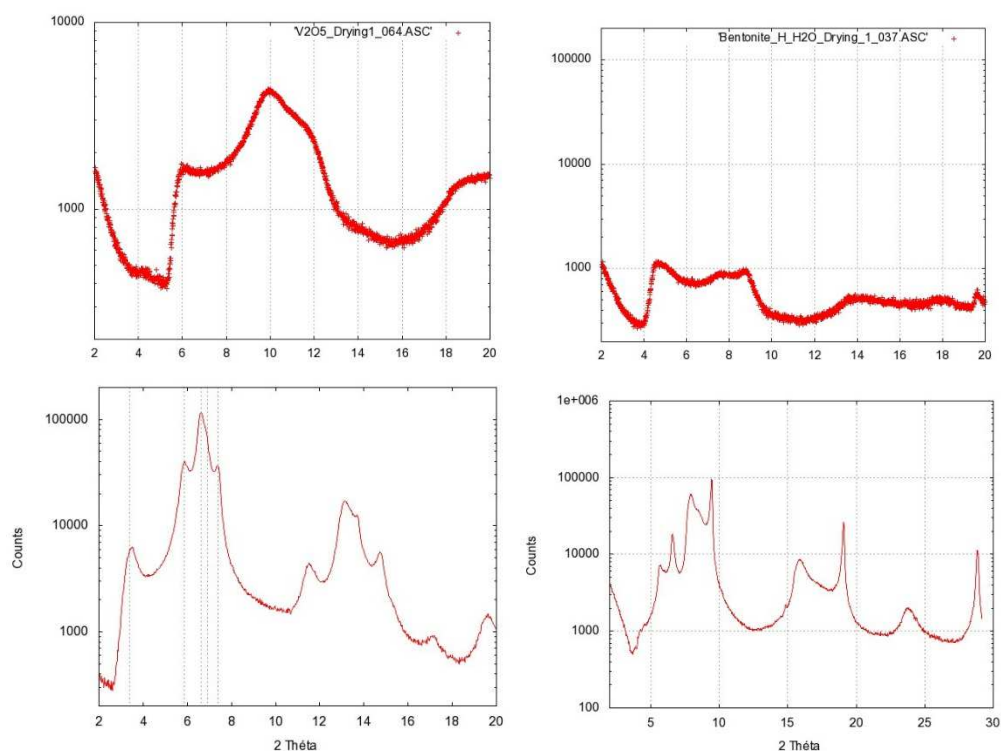
Lamellar phase exfoliation.

Coll. J.C. Gabriel (INAC)

Ordering 2D colloidal particles at the nanometer length-scale is currently a challenging and active research area in materials science. Ordering at the nanometric length scale can spontaneously appear when anisotropic objects form liquid-crystalline phases. Well known for organic species, this tendency lamellar phases were reported for clay particles, graphene and graphene oxide, or niobates but so far, no columnar phase was ever described for such objects. Among nanosheets, some phosphoantimonate single layers were shown to display a liquid-crystalline lamellar phase¹ (Figure) comprised of planar solid-like sheets (i.e. in which all atoms involved in a layer are covalently bonded) dispersed in water. Upon dilution, the lamellar spacing could be increased 100 fold, leading to 1D periodicities tunable from 1.5 to 225 nm. This behavior has also been observed for niobates and phosphates, but other very similar materials, or even clay and graphene nanosheets only self-assemble into nematic phases. The

physical origin of such a difference in behavior remains largely unknown so far but might be ascribed to differences in sheet size, rigidity, polydispersity, and/or interaction potentials.

Our general objective for this project is to understand why some nanosheets form lamellar phases whereas others only display nematic phases. For this, various inorganic phases have been exfoliated and studied both by SAXS and XRD. At very high concentration, various behaviors and structures have been then observed, depending on the materials, which indicates a strong dependence of water ordering on the chemical composition of the material studied.



XRD diagram showing high concentration water ordering of various layered materials.

¹Gabriel, J.-C. P., Camerel, F., Lemaire, B.J., Desvaux, H., Davidson, P., Batail, P. Swollen Liquid-Crystalline Lamellar Phase Based on Extended Solid-Like Sheets. *Nature* **413**, 504-508 (2001).

Metrology

Patterned membranes.

Coll. LETI/DTSI/SPAT/LLIT

SAXS measurements were carried out on a patterned sample: a network of tungsten lines deposited on a 50 nm thick Si membrane (see Figure 1). The width of the W lines is about 100 nm and the network period is 100 nm. The patterned sample area is 3 x 3 mm². The diffraction image was recorded with the detector at 4 m from the sample and showed a series of well-resolved diffraction peaks corresponding to (00l) reflections (see Figure 2). This study also shows the possibility of dimensional control in CD-SAXS for applications in nano-lithography to control network period and roughness of the flanks by analysis of the diffusion profile.

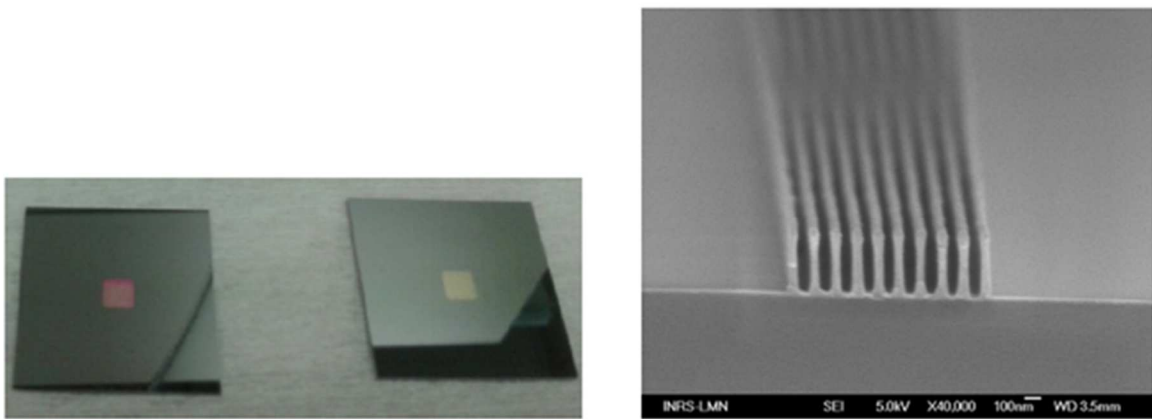
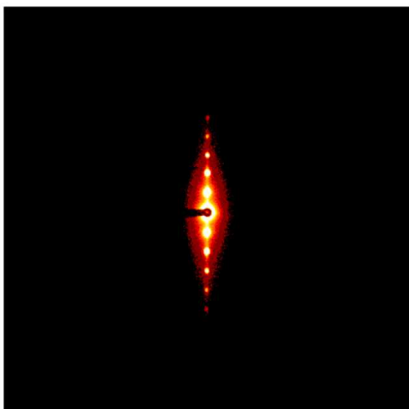


Figure 1. Tungsten line network deposited on ultra-thin silicon membranes (Courtesy by P. Gergaud and C. Constancias).

a)



b)

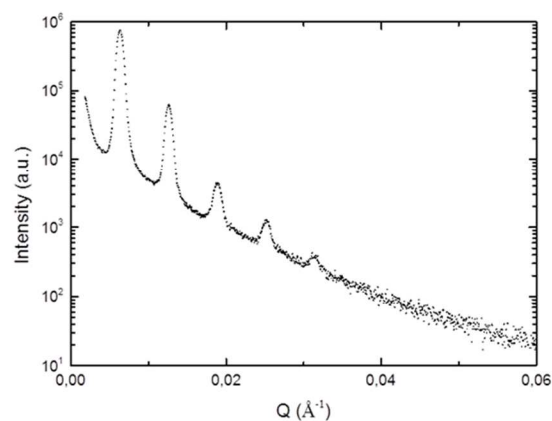


Figure 2. (a) SAXS image measured with the VANTEC-2000 detector for a W-line network of period 50 nm using a sample-detector distance of 4 m; (b) spectrum obtained after 2D - 1D data reduction